fractal and fractional

MDPI

Review

Models for Simulation of Fractal-like Particle Clusters with Prescribed Fractal Dimension

Oleksandr Tomchuk [1,2]

[1] ISIS Neutron and Muon Source, Rutherford Appleton Laboratory, Harwell Oxford, Didcot OX11 0QX, UK; oleksandr.tomchuk@stfc.ac.uk
[2] The Henryk Niewodniczański Institute of Nuclear Physics, Polish Academy of Sciences, 31-342 Kraków, Poland

Abstract: This review article delves into the growing recognition of fractal structures in mesoscale phenomena. The article highlights the significance of realistic fractal-like aggregate models and efficient modeling codes for comparing data from diverse experimental findings and computational techniques. Specifically, the article discusses the current state of fractal aggregate modeling, with a focus on particle clusters that possess adjustable fractal dimensions (D_f). The study emphasizes the suitability of different models for various D_f–intervals, taking into account factors such as particle size, fractal prefactor, the polydispersity of structural units, and interaction potential. Through an analysis of existing models, this review aims to identify key similarities and differences and offer insights into future developments in colloidal science and related fields.

Keywords: fractal dimension; particle cluster; simulation; generation algorithm; Monte Carlo; population balance equations; Langevin dynamics; diffusion limited aggregation; reaction limited aggregation

Citation: Tomchuk, O. Models for Simulation of Fractal-like Particle Clusters with Prescribed Fractal Dimension. *Fractal Fract.* **2023**, *7*, 866. https://doi.org/10.3390/fractalfract7120866

Academic Editor: Junjie Wang

Received: 29 October 2023
Revised: 22 November 2023
Accepted: 29 November 2023
Published: 5 December 2023

1. Introduction

The fractal theory [1] has found its wide application in many areas of science, including growth processes [2], surface roughness [3], viscosity [4,5], geophysics [6], polymers [7], as well as technology, including mineral extraction [8], environmental protection [9], drying technology [10], aerosol synthesis [11,12], solar geoengineering [13], composite material [14], cellular morphology [15], drug delivery [16], stock markets [17], etc. Various fractal and multifractal approaches are actively used to describe disordered branched systems in terms of structure or connections. In the generally accepted concept of the scientific search for the structure–property relationship, fractal modeling is certainly important both for direct problems, when a given scale-invariant microstructure determines the macroscopic properties of a physical system, and in inverse problems, which are devoted to restoring fine details of the structure by analyzing macroparameters.

Fractal geometry in particular was used to develop a better understanding of aggregation kinetics and physical properties in micro- and nanostructured materials (Figure 1). The fractality of aerogels, colloidal sols, emulsions, porous systems and so on is determined by the fact that they can be represented as irregular agglomerates of fine particles [18–22]. The exceedingly low densities observed in certain systems may be explained based on a hierarchy of aggregates-within-aggregates [23]. It is the features of physicochemical processes at the stage of synthesis which lead to the fact that materials are characterized by self-similar or self-affine structural correlations on many scales. It is the dissimilarity with quasi-homogeneous media that distinguishes them from the traditional multiphase composite systems, which are locally homogeneous in significant parts compared to the total size of the system. At the present much of our understanding of the structure and properties of fractal aggregates has come from computer simulations [24]. Consequently, modeling the structure of such fractal aggregates (agglomerates or clusters) is of genuine

interest since a detailed description of the morphology makes it possible to compare the results of different methods.

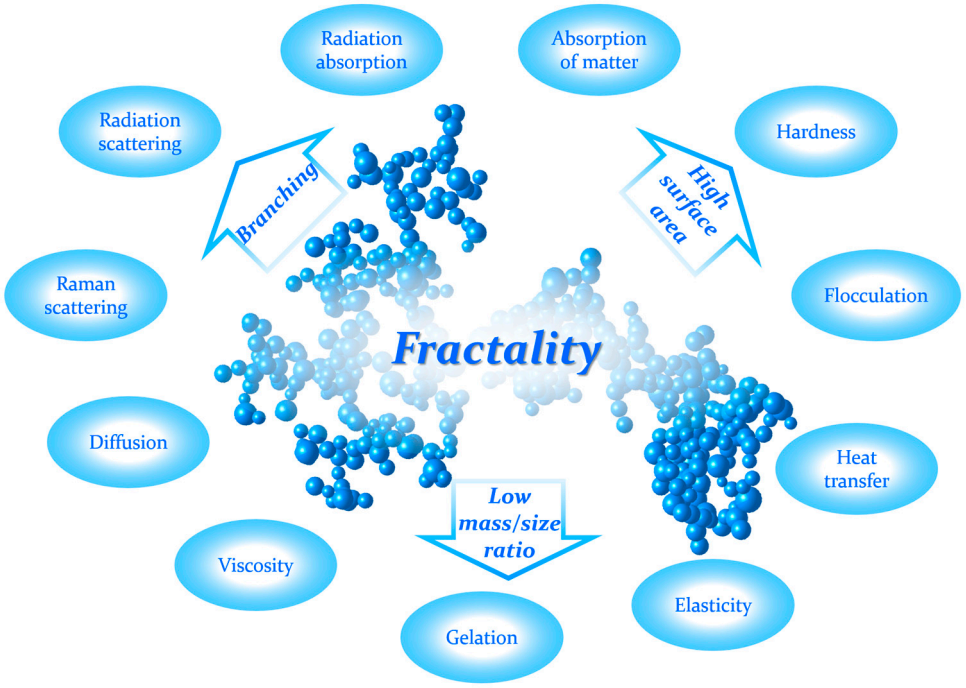

Figure 1. Physico-chemical properties affected by the features of the fractal structure of nanoparticle clusters.

Most observed mesoscale fractals are self-similar. Their fractal dimension, D_f, can be determined either from the mass–radius relation:

$$N = k_f (R_g/R)^{D_f}, \quad (1)$$

or from the behavior of density, ρ, autocorrelation function at intermediate distances, $R < r < R_g$:

$$\left\langle \rho\left(\vec{r}'\right)\rho\left(\vec{r}+\vec{r}'\right)\right\rangle \propto r^{D_f-3}, \quad (2)$$

where R_g is the gyration radius of an aggregate containing N particles of radius R (or characterized by mean radius $\langle R \rangle$) [1]. The fractal prefactor, k_f, is a dimensionless constant of the order of unity. It is a local characteristic dependent on the distribution of empty areas within the aggregate. By Mandelbrot k_f parameter is approximately inversely proportional to lacunarity [25,26]. Along with the common approaches for calculating the fractal dimension (Equations (1) and (2)), it is worth noting many others [1,8].

Today, various methods are used to study fractal clusters incorporated into media in various states of matter [27]. Experimental techniques are based, for example, on the scattering of various types of radiation, including visible light, X-rays and thermal neutrons [28–30], microscopic techniques [31,32], the study of aerodynamics [33–35], rheological research [36] or the adsorption of small particles [37,38]. In addition to the value of the fractal dimension, D_f, the sizes of aggregates and their structural units, the fractal prefactor, and some other parameters can be determined. As an alternative, approaches to the three- [39] or five-parameter [40,41] description of fractal clusters are presented in the literature. Even so, some model assumptions are often needed to extract structural information. The pool of models of fractal clusters and their correspondence to certain types of physicochemical synthesis processes is an important tool for precision structural analysis.

Historically, the first such model was Diffusion Limited Aggregation (DLA) [42,43]. The simplest principles of the growth algorithm, based on the alternate attachment of diffusing particles to the seed, gave a striking resemblance to a number of clustering phenomena, primarily in terms of the value of the fractal dimension parameter ($D_f = 2.5$ in

three-dimensional space). Since natural and artificially created fractal clusters of particles can have a fractal dimension in the entire range of connected systems, $1 \leq D_f \leq 3$, active development of models capable of giving different dimension values began in the 1980s. The next step was to abandon the sequential approach, which is valid for highly dilute systems, in favor of the simultaneous diffusion of all particles in the system. So, within the model of Diffusion Limited Cluster Aggregation (DLCA) [44,45], particles move along Brownian trajectories, and when they meet another particle or cluster, they join it. Thus, small clusters formed at the initial stage are assembled into larger ones, and so on. The algorithm provides for a slowdown of the movement of the cluster with mass, M. The translation diffusion coefficient is proportional to the M^{-1/D_f} factor. As a result, one cluster is generated containing all the particles in the system and having a fractal dimension within the range 1.74–1.86 [46]. If the sticking probability for particles/clusters is set to be less than unity, this leads to denser fractal structures, since it becomes possible to somewhat penetrate deep into the aggregate due to non-100% attachment to the periphery. This idea was implemented within the framework of the Reaction Limited Cluster Aggregation (RLCA) algorithm [47–50], which is characterized by $2 \leq D_f \leq 2.1$ values. In addition to the variation in the probability of sticking, the scientists also took the path of analyzing the influence of the motion trajectory on the resulting structure of the aggregates. Replacing Brownian trajectories with multidirectional rectilinear motions formed the basis of the Ballistic Limited Aggregation, namely BLA and BLCA models [51], which makes it possible to achieve $1.89 \leq D_f \leq 2.95$. Also, restructuring approaches were applied to the already generated clusters, which somewhat increased the value of the fractal dimension [52]. In addition, fractal properties were found in polymeric materials [53], percolation systems [8], surface roughness [3] and in the vicinity of critical points on the state diagram of various substances, which indicated new possibilities for exclusive approaches to modeling micron and submicron fractals of various D_f values [54,55].

All these undoubtedly important milestones in the science of modeling fractal clusters are described in detail in the remarkable reviews of the end of the last century (see, for example, [24,56–60]). These publications gave a systematic idea of the relationship between the kinetics of the process and the resulting fractal properties and even made it possible to divide algorithms into conventional "universality classes" in accordance with the value of the fractal dimension. For instance, the structures formed by cluster–cluster aggregation via either Brownian or linear trajectories probably lie in the same universality class which is distinctly different from that associated with the diffusion limited particle-cluster aggregation [61].

However, such a simplified view of the problem somewhat overlooked systems with D_f values that do not correspond to classical models. Moreover, in experiments, there are cases of a continuous change in the fractal dimension of already formed particle aggregates, which clearly cannot be described by the synthesis kinetics [62–64]. Incidentally, the approaches of limited diffusion or ballistics themselves are quite time-consuming to generate a representative array of clusters, which additionally stimulated the development of new approaches. The substantial interest on the part of various scientific and technical fields demanded that the shape of particles [65], their size distribution over a certain range [21,66–68] and boundary conditions [69] be included in the consideration. However, the main parameter to which attention is paid, and which is sought to be modeled close to the experimental value, remains the fractal dimension, D_f [1,70].

The description of experimental data, on the one hand, and the prediction of physical properties, on the other hand, require approaches in which it is possible to simulate a fractal cluster with any predetermined dimension (Figure 2). In this review, I am trying to look at the latest achievements in the field of modeling fractal clusters from the viewpoint of the possibility of controlling the fractal dimension value as an input model parameter within the framework of one or a few similar algorithms. The focus is primarily on self-similar fractals, as the most common in practice. I review the most popular numerical models, briefly comparing the fundamental differences in the underlying mathematical

or physical principles. The question under consideration is how wide the range of D_f can be covered using one or another generation algorithm. Particular attention is paid to the possibility of controlling additional structural parameters and estimates of computer time consumption. Thus, the comparison given in the article allows one to choose an algorithm for constructing fractal aggregates that will satisfy requests in terms of compliance with the scientific problem and implementation convenience. Given the constantly growing array of topical publications, a critical analysis of this kind seems necessary and timely.

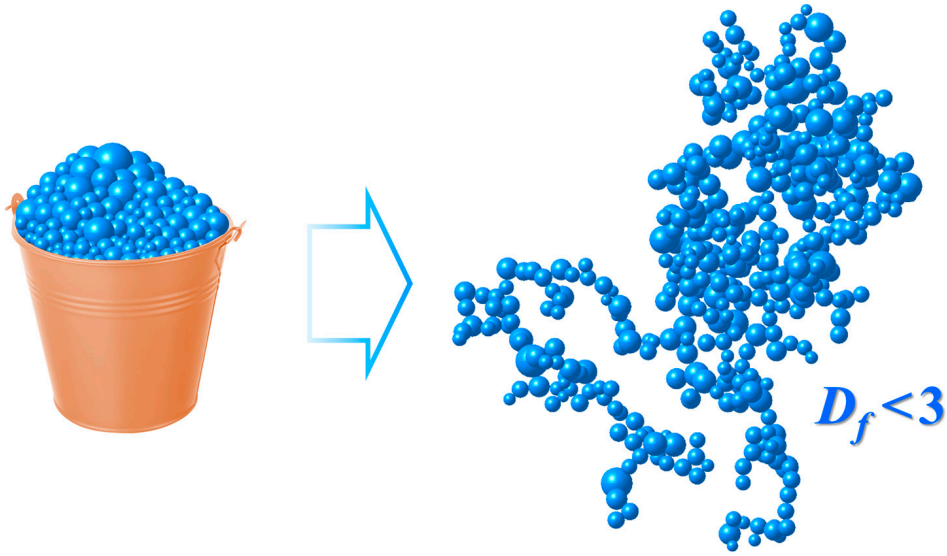

Figure 2. Visualization of the principal question of the review: how can a cluster of particles with a predetermined fractal dimension be assembled?

An important disclaimer is that this review concerns primarily stochastic fractal models, which most closely describe the objects observed in the experiments. That is, I deliberately exclude deterministic fractals from consideration. A detailed description of their certainly interesting properties can be found elsewhere [1,28,71–73].

I start the list of models with population balance equations (Section 2.1). Then, the results of modeling based on the Langevin equation (Section 2.2) are considered. In Section 2.3, I outline the current state of the numerical generation of fractal clusters using various modifications of the classical Monte Carlo approaches described above. A significant block of models concerns the geometric construction of fractal clusters with a predetermined fractal dimension by a hierarchical assembly of structural units, maintaining the specific mass–size ratio at each stage of simulation (Section 2.4). Models of topologically linear fractals are also considered to some extent (Section 2.5). Section 2.6 is devoted to some selected examples of the fractal aggregation modeling. Finally, possible research directions and open challenges are pointed out in summarizing part.

2. Fractal Cluster Models

Considerable effort has been devoted to the development of realistic models to simulate specific experimental results. They are listed below in this section.

2.1. Population Balance Equations

Population balance equations method describes the kinetics of aggregation and size distribution. It is based on the generalized Smoluchowski equation [19,74,75]:

$$\frac{dn_k}{dt} = \frac{1}{2}\sum_{j=1}^{k-1} \beta_{k-j,j} n_{k-j} n_j - n_k \sum_{j=1}^{\infty} \beta_{j,k} n_j, \quad (3)$$

where n_k is the concentration of clusters of size k, and $\beta_{j,k} = \beta_{j,k}\left(D_f\right)$ is the dimension-dependent aggregation kernel for two clusters of sizes j and k that determines features of kinetics through the probability of particle collisions. These kernels are also dependent on the particle's morphology, the flow regime, the viscosity of the carrier and the temperature. The solution of the system of coupled ordinary differential Equation (3) using appropriate discretization techniques gives the evolution of size distribution function.

The Smoluchowski equation was developed primarily for coalescence phenomena, but it has been adapted extensively to describe different particle aggregation processes. This method is widely used for simulating particles agglomeration, as it allows time-dependent structural phenomena to be followed and provides a quantification of the influence of the fractal dimension value. However, the population balance equations approach is not suitable for studying the morphology of clusters, particularly considering that no universal kernel exists. The proposed analytical expressions for $\beta_{j,k}$ must be constantly compared with experiments. These are significant limitations relative to the main goal of this review—modeling the structure of fractal clusters.

Nonetheless, the corresponding mathematical apparatus is constantly developing and finds its application in the physics of fractal systems. Improved population balance equations were proposed (e.g., refs. [74,76,77]) to refine the numerical accuracy, stability and computational efficiency. Multiple available models have been reviewed [78].

2.2. Langevin Dynamics and Its Derivatives

The Molecular Dynamics technique involves the simulation of a model system of interacting molecules by numerically integrating Newton's laws of motion [19]. However, for investigations of aggregating colloidal systems, where the characteristic timescale of particle motion is much greater than that of solvent molecular motion, alternative numerical techniques should be considered as more appropriate. For example, these can be various versions of Langevin Dynamics: Brownian Dynamics or Stokesian Dynamics. Both simulation types provide a full description of the N particles motion by solving the Langevin equation [20]:

$$m_k \ddot{\vec{r}}_k = \sum_{j=1}^{N} \vec{F}_{k,j}\left(\vec{r}_{ij}\right) + \vec{F}_k^{\mathrm{B}} - \vec{F}_k^{\mathrm{D}}, \tag{4}$$

where m_k and $\ddot{\vec{r}}_k$ are the mass and the acceleration of the k-th particle, respectively; $\vec{F}_{k,j}$ is the interparticle force; $\vec{F}_k^{\mathrm{B}}$ is the Brownian stochastic force acting on the k-th particle (the random kicks from collisions with solvent molecules); $\vec{F}_k^{\mathrm{D}}$ is the external force acting on the k-th particle (first of all, the viscous friction opposing particle motion); and particle inertia is neglected. In a situation where the primary particles become joined together into rigid clusters, the scalar diffusion coefficient may be replaced by a size-dependent coefficient corrected by factor ${n_k}^{-1/D_f}$ [20,79]. Many other physicochemical factors can be explicitly taken into account.

Both methods treat the solvent in a continuum approximation via the addition of stochastic forces. In the case of Stokesian Dynamics hydrodynamic interactions among particles are rigorously accounted for [80,81]. Stokesian Dynamics refers to the numerical simulation of the dynamic behavior of non-dilute suspensions under conditions in which hydrodynamic interactions make a predominant contribution to macroscopic properties such as rheology or sedimentation. In the case of the prevalence of effects of the random kicks from collisions with solvent molecules, and the viscous friction opposing particle motion, the formalism of Brownian dynamics is used [82]. Nevertheless, for the Brownian Dynamics formalism, Equation (4) can be extended to consider hydrodynamic interactions within the Ermak–McCammon algorithm [83] or the Heyes–Mitchell approach [84].

Time-consuming calculations in Langevin Dynamics are the price for a precise description of the cluster formation in real time. In contrast to the Population Balance Equations

approach, detailed structural information about the resulting aggregates is available. The fractal dimension, D_f, and the fractal prefactor, k_f, can be calculated through Equation (1). However, modeling clusters with a predetermined fractal dimension using Langevin Dynamics is manageable but not obvious.

Another Langevin-equation-based method for simulating colloidal particle aggregation is Dissipative Particle Dynamics, for which the fluid medium between the colloidal particles is modeled as an assembly of small particles which act as momentum carriers [85,86]. That sort of coarse-grained representation of the hydrodynamic medium leads to an effective short-range attraction induced by the structuring of the small fluid particles in gaps between closely approaching colloidal particles that complicates the simulation of colloidal dispersions. Again, when working with such a formalism, it is difficult to unambiguously prescribe the desired dimension of the final fractal aggregates.

Ferri et al. proposed a purely geometric aggregation morphological model able to mimic the aggregates arrangement obtained with a Brownian Dynamics simulation, wherein the fractal dimension is tuned between 1.2 and 3 with two compactness parameters [87]. These parameters describe the probabilities of the preliminary disposition of the subsequently attached particle relative to the potential attachment site (α), as well as potential attachment sites relative to the center of mass of the aggregate ($\beta \leq \alpha$). Brownian Dynamics results are used to parametrize this model, in order to constrain the morphology of the aggregates created. The given morphological model builds single aggregates of particles of any shape, replicating the Brownian Dynamics aggregates successfully (Figure 3). The particles are either in contact or at a controlled distance. The simplified version of the generation process is also proposed for the case of monodisperse spheres on a discrete grid. For this case, the strategy for the parametrization of the aggregation algorithm is presented in detail. The limitations of the technique are related to the fact that for large aggregates the available range of fractal dimensions is somewhat reduced (for $N > 40$ it is $2 \leq D_f \leq 3$).

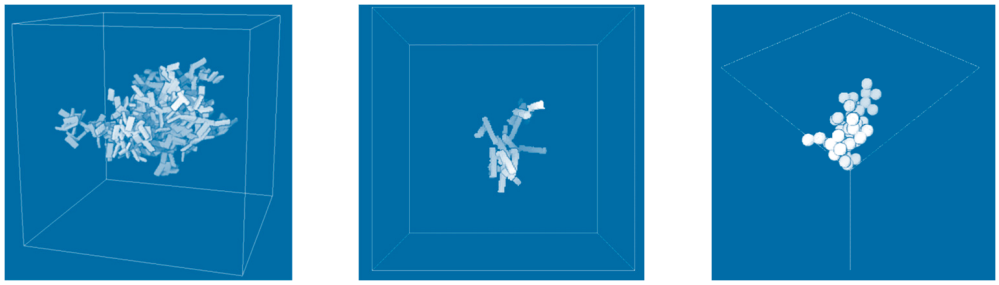

(**a**) (**b**) (**c**)

Figure 3. Simulation of aggregates using morphological model of Ferri et al. [87]: (**a**) platelets of size ratio of 20:8:3 and compactness parameters $\alpha = 0.1$, $\beta = 0.05$; (**b**) cylinders with height/diameter ratio of 5, $\alpha = 0$, $\beta = 0$; (**c**) spheres, $\alpha = 0.1$, $\beta = 0.05$.

However, Langevin Dynamics is rather computationally expensive [19,88]. On the other hand, the classical Monte Carlo methods (diffusion, ballistic and reaction limited aggregation models) given below are faster but limited by the simplified iterative particle dynamics and to the specific agglomeration regimes.

2.3. Monte Carlo Techniques

2.3.1. Modifications of DL(C)A

Monte Carlo (MC) models follow the structural evolution of an agglomerating system. Typically, a given number of primary particles is randomly placed in a three-dimensional space and allowed to move and "interact" according to specific rules, including probabilities. At the end of the simulation, a population of clusters with a given morphology is obtained. It is possible to estimate D_f as well as the fractal prefactor, k_f, by employing Equation (1). Notably, these simulations face limitations in the replication of aggregation processes involving interactions beyond the scope of potential functions, including hydrodynamic

effects such as hydrodynamic interactions or shear-induced aggregation [20]. In contrast to Langevin Dynamics, which is commonly used to study the agglomeration of nanoparticles, the MC method relies on an artificial description of time, making it difficult to obtain a physical description of the agglomeration process [19,22].

In the aggregation of particle–cluster models, the trajectory plays a decisive role, in contrast to cluster–cluster models [61]. DLA leads to structures with a considerably smaller fractal dimension than particle–cluster aggregations via linear particle trajectories, namely BLA. The effective dimension of particle–cluster aggregates can be continuously varied between the limits of the DLA and BLA models with the exponent, which describes the distribution of step lengths in the Levy-flight trajectory [89]. The impact of Brownian motion on the structure of aggregates resulting from cluster–cluster aggregation is much more diminutive, because the clusters cannot penetrate each other by means of any trajectory.

Accounting for some factors can affect the value of D_f in comparison with classical values pointed out in the Introduction section for the MC algorithms [60,90]. These include important improvements such as the consideration of the effects of cluster restructuring [52,91], flexibility [92], the effects of inter-particle interactions [57,93,94], etc.

The modified two-dimensional hierarchical model for cluster–cluster aggregation, incorporating partial reorganization following initial cluster contact, was investigated [91]. After two clusters contacted each other, one cluster was allowed to rotate about the center of the contacting particle in the other cluster until a second bond is formed. In some cases, the second cluster is also allowed to rotate to form a third bond. The results showed that the inclusion of rotational effects led to significantly increased cluster compactness at short length scales, with only a marginal increase in fractal dimensionality on longer scales ($\Delta D_f \leq 0.05$). Findings from both Brownian and linear trajectory aggregations were presented. Thereafter, the effects of basic restructuring mechanisms on cluster geometry in diffusion-limited, ballistic, and reaction-limited cluster–cluster aggregation were explored more precisely using three-dimensional off-lattice models, revealing comparable increases in fractal dimensionality ($D_f = 2.09$ for DLCA (Figure 4); $D_f = 2.25$ for RLCA) [52]. To achieve the fractal dimension of about 2.5, additional restructuring processes are required, involving the bending and twisting of particle loops and/or fragmentation with cluster reformation.

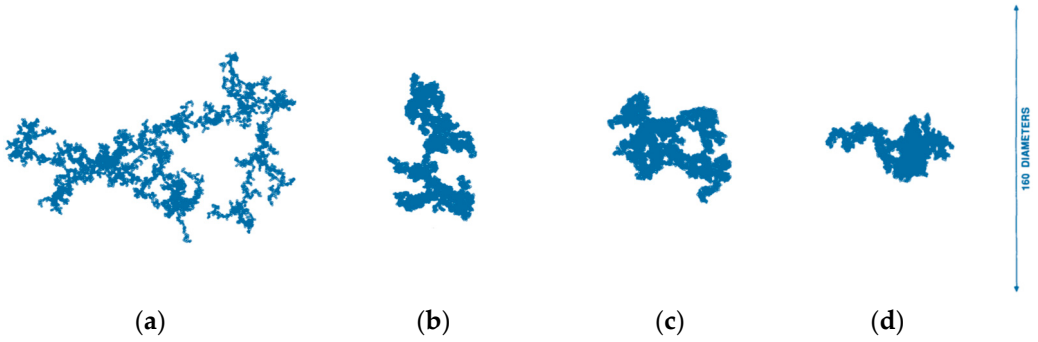

Figure 4. Three-dimensional DLCA clusters of almost 6000 particles with no readjusting rotations (**a**) and with one (**b**), two (**c**) or three (**d**) readjusting rotations after the initial contact. The four clusters are shown on the same scale. Adapted with permission from ref. [52]. 1988, AIP Publishing.

Another type of cluster restructuring has also been proposed for the three-dimensional hierarchical cluster–cluster aggregation models [95]. In these algorithms, it was assumed that contacts between pairs of particles once formed cannot be broken but may move on the surface of particles in one cluster which come into contact with particles in another cluster. Such structural readjustment processes increase the fractal dimension up to 2.13 and 2.21 for DLCA and BLCA, respectively. As in the previous case, the most striking changes occur at the first level of restructuring (Figure 5). In general, restructuring has a

more important effect on the short-range structure of simulated agglomerates than on the long-range morphology, which determines their fractal dimension.

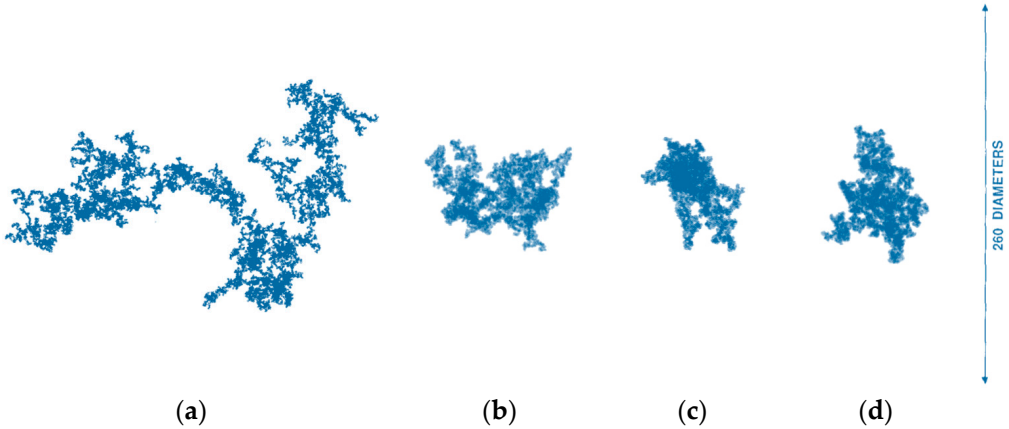

Figure 5. Three-dimensional BLCA clusters of 2^{14} particles with no readjusting rotations (**a**) and after first (**b**), second (**c**) and third (**d**) stages of restructuring, respectively. The four clusters are shown on the same scale. Adapted with permission from ref. [95]. 1988, Elsevier.

The DLCA model was modified by including cluster deformations using the bond fluctuation algorithm [92]. In addition to rigid motions of clusters, some internal movements are introduced with a controlling flexibility parameter. It was shown that including cluster deformations significantly alters the aggregation properties: a sol-gel transition was obtained at a given threshold value of the volume fraction. Below the threshold value, the intra-aggregate bonding prevails over the formation of a gelling network. On the other hand, above the threshold, the sol-gel transition occurs at a certain finite time. The fractal dimension of the aggregates forming the gel is very close to 2, as seen both from box-counting calculations and the mass–radius ratio.

DLCA morphology was studied as a function of structural unit overlap [96]. The morphology is parametrized by both the fractal dimension, D_f, and the fractal prefactor, k_f. For clusters built on a three-dimensional cubic lattice $D_f = 1.8$ and $k_f = 1.3$ were found for the spherical monomers in point contact. Both these values increased as overlap increased. The fractal dimension value reached 2. Structural features of the two-dimensional projections of these clusters were also precisely considered to analyze the relationship between the longest length and projected area as functions of monomer overlap [96].

The effects of rotational diffusion on off-lattice cluster-cluster aggregation have been investigated [97]. The effects of rotational diffusion continuously decrease D_f from a characteristic DLCA value. In the limit of a very high rotational diffusion rate compared to translational diffusion, the fractal dimension equals 1. It was mentioned that in most real physical systems, the diffusion constant ratio (the mean square displacement of the most distant point in the cluster due to rotational motion divided by the mean square displacement due to translational motion), will probably lie in the range 0–1, and the effect of rotational diffusion will be relatively small.

Statistical properties of growing DLA clusters were compared in the case of the fixed cluster, and in the case when the growing structure has a nonzero rotation around its initial seed [98]. It was shown that for a small enough rotative speed, the fractal dimension is growing as a function of cluster size, but for higher speed, it tends to the unity.

Various alternatives for calculating the probabilities of particle displacements in MC simulations were compared when agglomeration occurs in the DLCA regime [99]. An interpolating formula to simulate the transition between the BLCA and DLCA regimes was developed [100]. Most studies assume that particles are displaced by a constant distance equivalent to the diameter of a monomer, regardless of their sizes. Several studies have taken into account displacements that vary with cluster size [101–103]. The Monte

Carlo Agglomeration Code (MCAC) method with justified probabilities of particles' movement, considering size-dependent displacements and the ability to bring a validated and consistent physical residence time both for individual particles and for the ensemble of polydisperse particles, was introduced [22]. Based on a binomial approach and the discretization of Langevin Dynamics trajectories of individual particles, the definitions of specific particle persistent distance ($\lambda_p = \sqrt{18D\tau}$, where D is the particle's diffusion coefficient, and τ is the momentum relaxation time defined as the ratio between particle's mass and friction coefficient), its corresponding time step ($\Delta t = 3\tau$) and subsequent probabilities for particle displacements were found. The model combines the advantages of MC, i.e., the ability to efficiently simulate the complex agglomerates with fractal dimensions in the range $1.62 < D_f < 1.88$ [104], and the advantages of Langevin Dynamics to account for physical dynamics.

The widespread use of the reaction limited models confirm the importance of studying short-range interactions. For example, active, moving, and rotating particles and clusters were studied in two-dimensional simulations [105]. Motile particles changed irreversibly into nonmotile ones upon collision with a nonmotile particle until the system turns into absorbing state where all particles are nonmotile. A crossover from fractal aggregates at low density ($D_f = 1.74$) to homogeneous ones at high density ($D_f = 2$) was found. The persistence of single-particle dynamics pushes this crossover to a higher density and can be used to change the porosity of the aggregate. At the lowest density the fractal dimension approaches that obtained in DLA.

Another approach involves introducing an effective aggregation radius of aggregated particles, Λ, for modeling short-range interactions in a frame of a particle–cluster regime [106]. A particle far from this region does not interact with the cluster until its trajectory intersects the interaction boundary of any aggregated particle (distance to the particles in the cluster is less than Λ) for the first time. Then, the position of the new particle in the cluster is determined near the closest previously aggregated particle. For $\Lambda = 1$, or direct-contact interaction, one obviously recovers the usual DLA or BLA models. However, for sufficiently large clusters $D_f \to 1$ as $\Lambda \to \infty$, and the entire range of $1 < D_f < 2$ and $1 < D_f < 1.71$ may be covered for ballistically limited and diffusion-limited aggregation regimes, respectively (Figure 6).

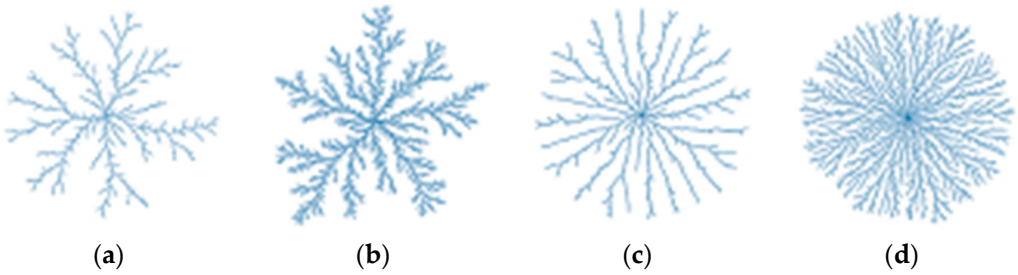

(**a**) (**b**) (**c**) (**d**)

Figure 6. DLA- (**a**,**b**) and BLA-based (**c**,**d**) aggregates with varying effective aggregation radius, Λ, and a fractal dimension of 1.31 (**a**,**c**) and 1.51 (**b**,**d**), correspondingly [106].

The consideration of long-range interactions between clusters also affects their fractal dimension [107], which is attributed to transparency effects [108]. Namely, the electrostatic interactions can reduce the cluster penetration and decrease the fractal dimension [93]. A physically justified extension of the DLCA model for a case of polarizable clusters emphasizes sticking by tips and gives $D_f = 1.42$ [93]. At the next stage, the hierarchical cluster–cluster aggregation model was extended by introducing dipolar interactions between the magnetic dipoles attached to each particle [94]. It was found that the fractal dimension of the resulting clusters decreases when the intensity of the momenta increases. It is worth noting that although slightly smaller, the fractal dimension recovered, $D_f = 1.34$, in the limit of very large momenta ("zero temperature" limit) is very close to the tip-to-tip model in three dimensions. The upper, "zero momentum" limit was found to be 1.72.

The irreversible aggregation of non-interacting particles and those interacting through repulsive and attractive potentials was investigated, explicitly incorporating the rotational diffusion of aggregating clusters (Figure 7) [90]. The findings demonstrate that particle attraction does not influence the aggregation mechanism or the structure of the aggregates, which remain comparable to those of non-interacting particles. Conversely, repulsive particles form denser aggregates, with an increase in both fractal dimension and aggregation times as temperature decreases. The structure of the aggregates from non-interacting particles depends on the ratio of rotational and translational diffusion coefficients showcasing an instance of DLCA for rotating clusters. In the case of repulsive particles, rotational diffusion plays a role in the formation of RLCA clusters. Comparing the fractal dimensions of non-rotating clusters of non-interacting particles and rotating clusters of repulsive particles elucidates the consistent values observed in the established DLCA model and experiments on colloidal particles.

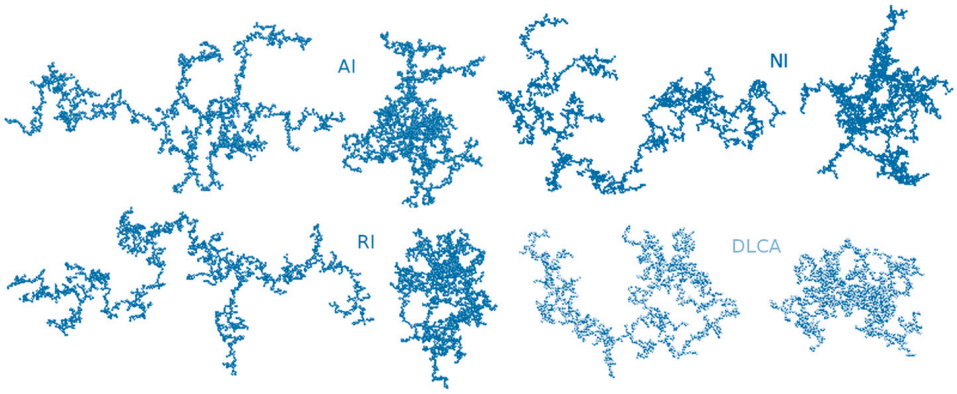

Figure 7. Representative clusters formed from the same initial configuration by the attractive (AI), repulsive (RI), and non-interacting particles (NI) with and without (DLCA) rotational diffusion [90].

2.3.2. Eden Model and Its Derivatives

The Eden model describes the growth of specific types of clusters such as bacterial colonies and the deposition of materials through the random accumulation of particles on their boundary [109,110]. The algorithm is essentially as follows. On a two-dimensional square lattice, a site is labeled as occupied by particle. Then, any one of the four possible adjacent cells is randomly chosen to be filled by the next particle. The pair now has six possible growth sites. The process continues until a cluster of certain size is formed. It is found that the cluster has a solid core, i.e., is compact. This is an example of a surface fractal. Several versions of the Eden model have been introduced that give similar but somewhat different boundary statistics depending on the probability distribution of the possible paths from occupied to adjacent unoccupied positions [111].

A three-dimensional off-lattice model, namely the Porous Eden Model, was proposed to generate fractal aggregate structures (Figure 8) as a variation of the Eden Model with the additional capability of randomly inactivating particles with a given inactivation probability, p [112]. As this probability increases from 0 to 1, the proposed generation model follows a continuous transition between different types of fractal structure, including an off-lattice Eden Model, a self-avoiding random walk model, and a linear chain with partially constrained growth directions.

Microstructural properties (the radius of gyration, shape factor, mass and surface fractal dimensions, specific surface area, porosity and pore size distribution) can be controlled by adjusting the inactivation probability and the number of particles. For example, mass fractal dimension can take values of $1.6 \leq D_f \leq 3$. In addition, the proposed approach is convenient to implement and has high computational efficiency.

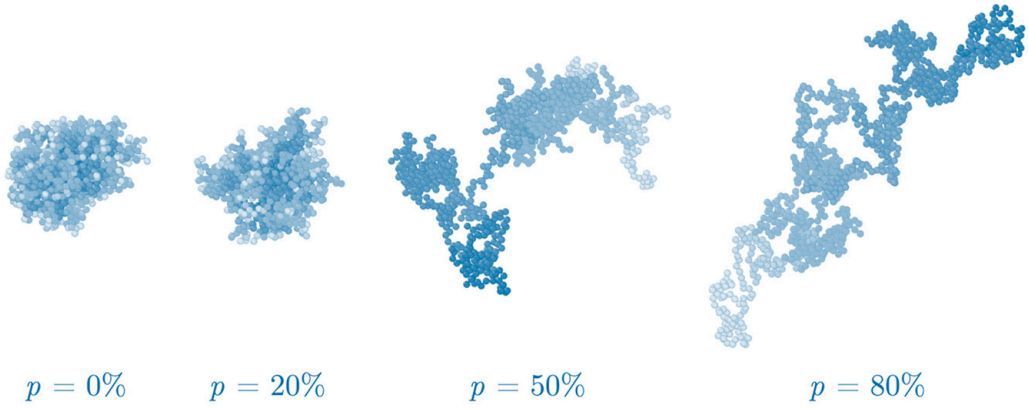

Figure 8. Typical aggregates of 1000 particles generated using the Porous Eden Model with increasing inactivation parameter, p. Adapted with permission from ref. [112]. 2019, Elsevier.

2.4. Hierarchical Assembly According to Mass–Radius Ratio

Recently, there has been a surge in the popularity of non-kinetic algorithms for the formation of fractal clusters through a hierarchical arrangement of particles. These algorithms aim to ensure strict adherence to fractal scaling at each iterative step. One notable instance of this adherence is observed in the mass–radius relationship (1). Although primarily rooted in geometric principles, these methodologies enable the continuous manipulation of the fractal dimension of the clusters. Consequently, these models find versatile application in the structural simulation of aggregates spanning a wide spectrum of sizes, ranging from the nano to the macro scale, owing to their independence from specific forces.

2.4.1. Monodisperse Particle–Cluster Models

A sequential particle–cluster algorithm for generation of aggregate geometry has been developed by Filippov et al. [113]. It allows for the adjustment of the structural parameters like D_f or k_f to prescribed values and consequently is widely used. In a frame of the given tunable particle–cluster generation algorithm, identical spherical particles are added iteratively under the condition that the scaling law (1) is fulfilled exactly at each step for predefined values of parameters involved. The iterative procedure could be represented by calculating the distance between the center of the N-th particle, $\vec{r}_N$, with the center of mass of the cluster already containing $N-1$ particles, $\vec{r}^{\,0}_{N-1}$:

$$\left|\vec{r}_N - \vec{r}^{\,0}_{N-1}\right|^2 = \frac{N^2R^2}{N-1}\left(\frac{N}{k_f}\right)^{2/D_f} - \frac{NR^2}{N-1} - NR^2\left(\frac{N-1}{k_f}\right)^{2/D_f}. \quad (5)$$

It is the case that the center of the next particle must be situated on the spherical surface determined by Equation (5), and it must be in point contact with any other particle of the cluster. Equation (5) is derived from the mass–radius relation (1), and the definition of the gyration radius, R_g, is corrected for the $N = 1$ limit, $R_g = \sqrt{a^2 + \frac{1}{N}\sum_{i=1}^{N}\left|\vec{r}_i - \vec{r}^{\,0}\right|^2}$ [113]. A similar algorithm was earlier described by Mackowski [114,115], but the restriction (5) has not been given explicitly. In such a way, it can be possible to cover the entire range of fractal dimensions of branched clusters in three-dimensional space, $1 \leq D_f \leq 3$. Examples of clusters of both types are shown in Figure 9a,b.

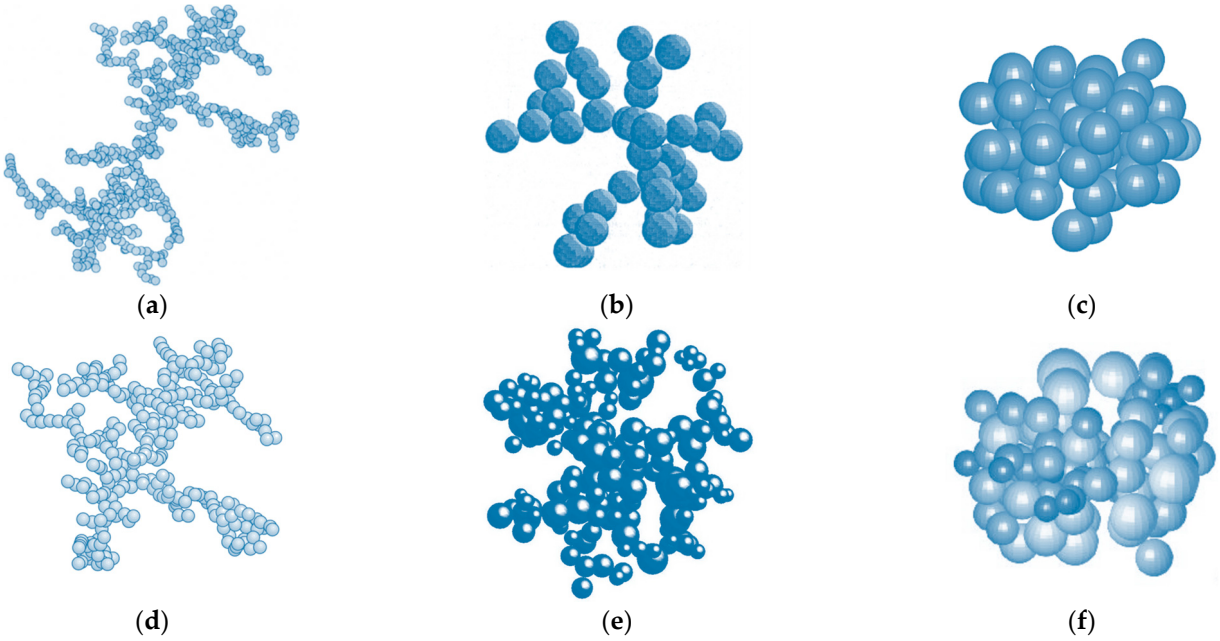

Figure 9. Typical particle–cluster fractal-like aggregates of monodisperse (**a**–**c**) and polydisperse (**d**–**f**) particles. (**a**) Sequential algorithm by Filippov et al., $D_f = 1.8$. Adapted with permission from Ref. [113]. 2000, Elsevier. (**b**) Sequential algorithm by Mackowski, $D_f = 1.9$. Adapted with permission from Ref. [115] © The Optical Society. (**c**) Tunable Sequential Aggregation-based model, $D_f = 2.81$. Adapted with permission from ref. [116]. 2020, Elsevier. (**d**) Polydisperse sequential algorithm by Dolotov et al., $D_f = 1.9$. Adapted with permission from Ref. [117]. 2007, Springer Nature. (**e**) Polydisperse sequential algorithm by Tomchuk et al., $D_f = 2.4$. Adapted with permission from ref. [118]. 2015, American Chemical Society. (**f**) The modified polydisperse Tunable Sequential Aggregation model, $D_f = 2.5$ [119].

The prefactor k_f usually displays uniform downtrends with the fractal dimension [120–122]. Nevertheless, for some aggregation processes, these are uptrends [123]. Attempts to explain these trends were made based on either the packing of spheres in space or a small N limit for clusters' structure. When N is small, the ways in which the monomers can assemble are of limited number and hence are not influenced by the aggregation scheme. Therefore, this correlation somewhat limits the simultaneous use of values of the parameters k_f and D_f.

Another tunable particle–cluster aggregation model was developed to construct the fractal-like agglomerates consisting of monodisperse spherical primary particles [116]. An approach of tuning the fractal dimension at a given fractal prefactor and porosity, ε, was used in a frame of previous algorithm [113]. The D_f–parameter can be adjusted with respect to the porosity correlation obtained by Singh and Tsotsas [124]:

$$\varepsilon = 1 - 0.465N\left(k_f/N\right)^{3/D_f}, \quad (6)$$

keeping the porosity and the number of primary particles the same. By tuning the fractal dimension with different prefactor in this way, the formed agglomerates look almost the same. Therefore, one can overcome limitations regarding the k_f values. The described algorithm is referred to as Tunable Sequential Aggregation (Figure 9c).

2.4.2. Polydisperse Particle–Cluster Models

The particle polydispersity is a common case in practical applications, so the introduction of particle polydispersity into the modeling of stochastic fractal aggregates extends the possibilities for studying correlations in natural and industrial fractal systems as well as modeling physical properties of different nanomaterials. The impact of particle polydispersity on the structure and dynamics during coagulation remains poorly understood.

Within the free molecular regime, the polydispersity of constituent particles does not significantly influence the asymptotic fractal dimension [31,68] as confirmed by subsequent research focusing on agglomerates containing tri-disperse particles in the continuum regime [125,126]. Conversely, it was demonstrated that an increase in particle polydispersity leads to more open structures [21]. Polydispersity characteristics have substantial implications for various static and kinematic features of the fractal agglomerates, including electron spin resonance [117], radiative properties [66,127], diffusion [128,129], dynamic light scattering [130,131], rheology [132], thermal conductivity [133], etc.

Special sequential algorithm for the generation of aggregates of polydisperse particles characterized by the preset values of the fractal dimensions and prefactor was developed [117]. The above-mentioned approach [113] was generalized to the case of polydisperse particles distributed over a certain range of radii and, consequently, masses:

$$\left|\vec{r}_N - \vec{r}^{\,0}_{N-1}\right|^2 = \frac{\langle m\rangle_N^2\langle R\rangle_N^2}{\langle m\rangle_N\langle m\rangle_{N-1} - \langle m\rangle_{N-1}^2}\left(\frac{N}{k_f}\right)^{2/D_f} - \frac{\langle m\rangle_N\langle R\rangle_N^2}{\langle m\rangle_{N-1}} - \frac{\langle m\rangle_N\langle R\rangle_{N-1}^2}{\langle m\rangle_N - \langle m\rangle_{N-1}}\left(\frac{N-1}{k_f}\right)^{2/D_f}, \quad (7)$$

where m_N is the mass of N-th particle and R_N is its radius, $\langle m\rangle_N$ is the average mass of the particle, and $\langle R\rangle_N$ is the mean radius of particles for aggregate composed of N particles. In the approach considered, the aggregate is constructed by the addition of single particles, the positions of which are set by the value of fractal dimension (Figure 9d).

A similar idea was implemented in terms of the mass of clusters, M_N [118]. In addition, the radius of gyration of the added spherical particle, $\sqrt{3/5}R_N$, was taken into account more correctly:

$$\left|\vec{r}_N - \vec{r}^{\,0}_{N-1}\right|^2 = \frac{M_N^2\langle R\rangle_N^2}{m_N M_{N-1}}\left(\frac{N}{k_f}\right)^{2/D_f} - \frac{3M_N R_N^2}{5M_{N-1}} - \frac{M_N\langle R\rangle_{N-1}^2}{m_N}\left(\frac{N-1}{k_f}\right)^{2/D_f}. \quad (8)$$

The result of this algorithm is presented in Figure 9e for 33% lognormal polydispersity.

The sequential tunable algorithm for generation monodisperse agglomerates [116] was improved and extended to polydisperse units [119]. The improved algorithm, Modified Polydisperse Tunable Sequential Aggregation (MPTSA), can completely retain the given input structural properties for polydisperse clusters. The standard deviation of the normal distribution of primary particle radius is limited to 10% of the mean value. A modified polydisperse tunable aggregation model has been developed using the expression to calculate the distance of the new approaching particle.

$$\left|\vec{r}_N - \vec{r}^{\,0}_{N-1}\right|^2 = \frac{M_N^2\langle R\rangle_N^2}{m_N M_{N-1}}N^{2/D_{f,t}} - \frac{3M_N R_N^2}{5M_{N-1}} - \frac{M_N\langle R\rangle_N^2}{m_N}(N-1)^{2/D_{f,t}}, \quad (9)$$

taking into account the correction $D_{f,t} = D_f\left(\ln\left(N_p\left(1-1/k_f\right)\right)\right)$, was introduced to overcome the fractal prefactor limitation in the construction of the aggregate of N_p particles [116]. Irrespective of each agglomerate having a tuned fractal dimension in the MPTSA model, fractal properties extracted for reconstructed agglomerates (Figure 9f) were closer to their predefined values than those provided by previous aggregation models [116,134].

Nevertheless, it was established that DLA agglomerates are definitely not self-similar [135–137]. Compared to small aggregates, the morphology of relatively large aggregates can be characterized as being far more compact. The correlation functions of DLA aggregates in both real and reciprocal space do not show simple scaling described by D_f-parameterized power laws in the corresponding ranges. These results do not exclude the fact that the DLA cluster remains fractal, but rather that it is not a self-similar fractal. Therefore, one must carefully use the approaches outlined in this section in modeling real systems, which are often self-similar. Even if it is possible to repeat the mass-size dependence of type (1), for the particle–cluster algorithms, it is possible to deviate from dependence (2).

2.4.3. Cluster–Cluster Models of Monodisperse Particles

Hierarchical assembly along the cluster–cluster path is much less subject to violation of self-similarity symmetry, since even qualitatively, it is clear that the structure is repeated locally in accordance with the model. Therefore, it is natural that these algorithms are increasingly used in multiple applied problems despite the relative complexity of implementation compared to particle–cluster approaches (e.g., refs. [130,131]).

The first hierarchical cluster–cluster aggregation model, tunable dimension cluster-cluster aggregation (tdCCA), was introduced, allowing for the building irregular fractal clusters on a three-dimensional lattice with any predefined fractal dimension ranging from 1 up to 2.55 [138]. The tdCCA algorithm works iteratively by sticking aggregates of the same number of particles at the correct distance between centers of mass in order to recover the desired scaling (1):

$$\left|\vec{r}_1^{\,0} - \vec{r}_2^{\,0}\right|^2 = 4\left(4^{1/D_f} - 1\right)\frac{R_{g1}^2 + R_{g2}^2}{2} + 1. \quad (10)$$

Later, tdCCA was adapted for the off-lattice generation of fractal clusters [139]. The procedure starts with a collection of 2^n particles grouped into pairs to obtain 2^{n-1} dimers. The dimers are grouped into pairs that generate tetramers and so on. An aggregate of the next generation is obtained by sticking together two aggregates of the previous generation containing equal number of particles. The procedure stops iterating when a final aggregate of 2^n particles is obtained (Figure 10).

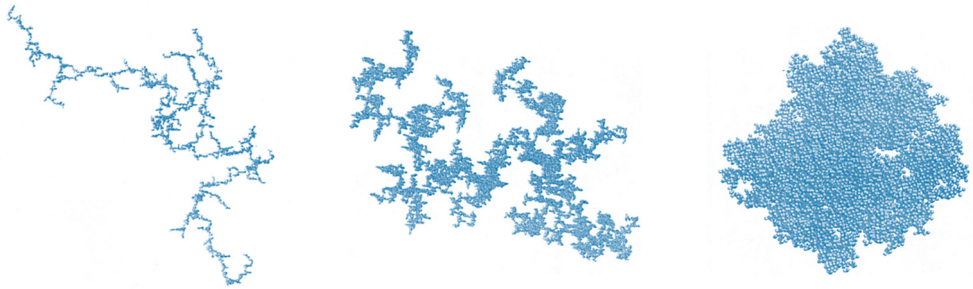

(**a**) (**b**) (**c**)

Figure 10. On-lattice aggregates containing 2^{14} particles each, with fractal dimension $D_f = 1.5$ (**a**), $D_f = 2.0$ (**b**), and $D_f = 2.5$ (**c**) generated with tunable dimension cluster–cluster aggregation model. Adapted with permission from ref. [139]. 1998, Elsevier.

A straightforward implementation of the tdCCA model requires computational effort scaling with $O(N^4)$ of the aggregation number. By applying two minor changes to the algorithm, the computational effort can be reduced to $O(N^2)$ [140]. The changes concern the introduction of MC-based methods into blocks for assessing the intersection and contact of clusters. Additionally, it allows for the efficient parallel implementation of the tdCCA algorithm but still in the range $1 \leq D_f \leq 2.55$.

The generation of clusters composed of rigid monodisperse primary particles with variable fractal dimension in the range from 2.2 to 3 was also reported [122]. Artificial clusters with variable fractal dimension were generated using a modified version of the tdCCA model for $2.2 \leq D_f \leq 2.5$ and a densification procedure including a Voronoi tessellation for $2.5 \leq D_f \leq 3$ (Figure 11a–d). This process of densification is executed in the following steps. Initially, a Voronoi tessellation is conducted on a given cluster. Subsequently, any Voronoi vertices that would result in the overlap of primary particles upon placement are disregarded. Following this, particles located farther from the cluster's center of mass are randomly relocated to fill the remaining holes, which are unoccupied Voronoi vertices, within the cluster's interior. The guideline for this repositioning is that the gyration radius decreases as a consequence of the particle's relocation within the cluster.

Upon the placement of a particle onto an empty Voronoi vertex, it is randomly adjusted to establish a connection with neighboring particles. As soon as particles have been allocated to all Voronoi vertices identified in the initial step, a subsequent Voronoi tessellation is conducted, and the particle exchange process continues. This sequence is reiterated until the condition of decreasing R_g can no longer be satisfied, ultimately resulting in a minimal possible radius of gyration and a fractal dimension of 3. Stopping the procedure earlier leads to intermediate values of the fractal dimension. For all generated aggregate populations, it was found that the aggregate mass and the aggregate size, characterized by the radius of gyration, follow a fractal scaling (1). Furthermore, the obtained prefactor of the fractal scaling, k_f, is related to D_f according to $k_f = 4.46 D_f^{-2.08}$.

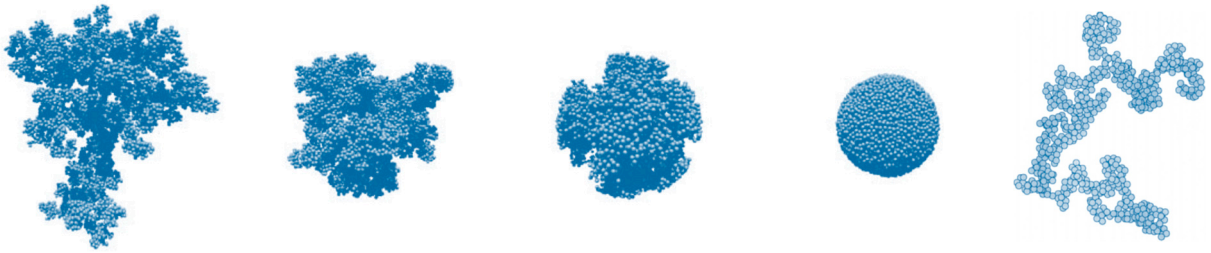

(**a**) (**b**) (**c**) (**d**) (**e**)

Figure 11. (**a**–**d**) Examples of aggregates of 10^4 particles with fractal dimension $D_f = 2.2$ (**a**), $D_f = 2.5$ (**b**), $D_f = 2.8$ (**c**), and $D_f = 3.0$ (**d**) obtained with the modified tdCCA model and the following densification via Voronoi tessellation [122]. (**e**) An aggregate of 724 particles with fractal dimension $D_f = 1.8$ generated using the tunable CCA algorithm. Adapted with permission from ref. [113]. 2000, Elsevier.

A more general algorithm was introduced [113], which allows the agglomeration of clusters with different numbers of primary particles. Hence, the final aggregation number is not necessarily a power of 2 like in tdCCA model. Equation:

$$\left|\vec{r}_1^{\,0} - \vec{r}_2^{\,0}\right|^2 = \frac{N^2 R^2}{N_1 N_2}\left(\frac{N}{k_f}\right)^{2/D_f} - \frac{N}{N_2} R_{g1}^2 - \frac{N}{N_1} R_{g2}^2 \tag{11}$$

yields a necessary and sufficient condition for fulfillment of the scaling law (1) by the resulting cluster of $N = N_1 + N_2$ particles. Based on this equation, the CCA algorithm combines small clusters pairwise, following an arbitrary hierarchical scheme. Each of the agglomeration events includes placing the centers of mass of two clusters to random points at a distance given by Equation (11) followed by their rotation until the combining clusters have at least one contact point (and no overlapping). The final result is one large aggregate, satisfying the fractal mass-radius ratio (1) exactly (Figure 11e).

The implementations of various computer models are mostly based on a trial-and-error procedure. Such approach is very time consuming. For example, in the literature some authors claim that to generate an aggregate composed of more than 1000 primary particles from hours to days are needed [130]. A very fast and accurate implementation of the tunable CCA algorithm was presented by Skorupski et al. [137]. Randomization is reduced to its necessary minimum and the position of a new cluster is calculated with algebraic methods. The algorithm is capable of generating a wide set of aggregates characterized by different morphological parameters. For example, to generate an aggregate composed of 2^{14} particles with $D_f = 1.8$ and $k_f = 1.3$ on a standard personal computer using the CCA routine, less than a minute is needed. It is worth noting that a method based on the particle–cluster aggregation processes was also considered.

2.4.4. Cluster-Cluster Models of Polydisperse Particles

Although the tunable CCA model by Filippov et al. was designed to generate only fractal-like aggregates of monodisperse primary particles, it is relatively easy to introduce polydispersity into algorithm of Skorupski et al. [137] replacing the fixed particle radius, R, with the averaged particle radius, $\langle R \rangle$. The calculation of the rotation angles should be altered accordingly, i.e., in all equations the distance between particle centers, $2R$, should be replaced with $R_1 + R_2$. Such an approach does not ensure the preservation of fractal dimension and fractal prefactor for every individual aggregate but only for an ensemble of a large number of aggregates.

A new algorithm, FracVAL (fractal aggregate generation algorithm developed in Valparaíso), again based on the tunable CCA algorithm was developed by using specific aggregation strategy for generating fractal clusters of polydisperse primary particles [141]. The algorithm is also able to preserve the prescribed D_f and k_f for each aggregate (Figure 12), regardless of its size and polydispersity (0–11% for lognormally distributed particles). The FracVAL algorithm is programmed in a hierarchical manner for aggregation between sub-clusters with approximately the same aggregation number.

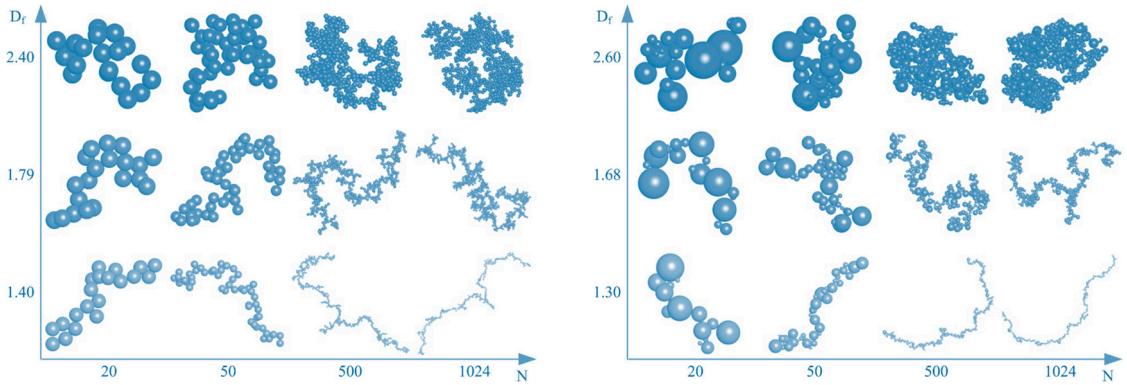

Figure 12. (**a**) Typical aggregates generated by FracVAL with monodisperse (**a**) and polydisperse (**b**) primary particles. Adapted with permission from ref. [141]. 2019, Elsevier.

The distance between the centers of mass of the two sub-clusters to be aggregated is calculated as:

$$\left| \vec{r}_1^{\,0} - \vec{r}_2^{\,0} \right|^2 = \frac{M^2}{M_1 M_2} \langle R \rangle_{N,g}^2 \left(\frac{N}{k_f} \right)^{2/D_f} - \frac{M}{M_2} \langle R \rangle_{N_1,g}^2 \left(\frac{N_1}{k_f} \right)^{2/D_f} - \frac{M}{M_1} \langle R \rangle_{N_1,g}^2 \left(\frac{N_2}{k_f} \right)^{2/D_f}, \quad (12)$$

where $\langle R \rangle_{N,g}$ corresponds to the geometric mean via relation $\log \langle R \rangle_{N,g} = N^{-1} \sum_{i=1}^{N} \log R_i$.

Since the positions of the two contacting primary particles and the mass centers of the two aggregating clusters are found using analytical expressions, FracVAL is considerably computationally efficient for generating fractal aggregates for different combinations of D_f, k_f and polydispersity. The algorithm is validated by analyzing the density–density correlation functions. The predefined fractal parameters are found to be accurately preserved for each individual aggregate. The performance of the proposed algorithm is evaluated for fractal aggregates consisting of up to 1000 primary particles and for fractal dimension variation over the entire D_f range between 1 and 3, and k_f range between 0.1 and 2.7. Aggregates consisting of 500 monomers are generated on average in a few minutes on a common personal computer, illustrating the efficiency of the FracVAL algorithm.

In a frame of considered cluster–cluster models [113,137,141], a particle–cluster aggregation algorithm is first used to obtain a set of small aggregates consisting of approximately 5–10 primary particles because the local structure at the length scales less than $< 10R$ a DLA-like aggregate is quantitatively similar to a DLCA-like aggregate [136], but particle–

cluster sequential algorithms are much more efficient because they are less subject to spatial constraints at small size scales.

A generalized non-kinetic off-lattice tunable cluster–cluster algorithm, proposed by Tomchuk et al. [121] for the construction of irregular fractal clusters of polydisperse particles, does not include a particle–cluster model in the early stages. At all iterations for all generations of sub-clusters, the generalized algorithm is cluster–cluster. The use of analytical approaches to calculate the coordinates of two sub-clusters when combined into one aggregate also increases the computational efficiency, as in the two methods described above. Another aspect concerns the fact that the generalized model is not limited to spherical particles but can also be used to construct fractal clusters of particles of any shape since it operates in terms of the gyration radii according to Huygens–Steiner theorem.

The procedure of the stochastic cluster generation starts with primary polydisperse particles distributed according to an arbitrary function. Expressions for R_g of most common primary particle shapes are well known [142]. As a first step, a part of them can be combined into dimers, using

$$R_g = \sqrt{\frac{M_1}{M} R_{g1}^2 + \frac{M_2}{M} R_{g2}^2 + \frac{M_1 M_2}{M^2} \left| \vec{r}_1^{\,0} - \vec{r}_2^{\,0} \right|^2} \tag{13}$$

to determine the gyration radius of every dimer. Thereafter the produced associations can be assembled pairwise following a hierarchical scheme with predefined parameters D_f and k_f. In each step, the centers of mass of two current clusters (the minimum possible combination is a dimer plus a monomer or a dimer plus a dimer) are placed at random points at a distance, as follows:

$$\left| \vec{r}_1^{\,0} - \vec{r}_2^{\,0} \right| = \sqrt{\frac{M^2}{M_1 M_2} \langle R \rangle_N^2 \left(\frac{N}{k_f} \right)^{2/D_f} - \frac{M}{M_2} R_{g1}^2 - \frac{M}{M_1} R_{g2}^2}. \tag{14}$$

Then, the clusters rotate until at least one contact between the primary particles of the clusters is achieved, thus excluding an overlap. There are several steps to do this. First, the condition of non-overlapping two sub-clusters is checked. If there is overlapping, the sub-clusters rotate along two mutually perpendicular axes, passing through the center of mass, at random angles until the intersection is eliminated. Then, a pair of particles from two sub-clusters is selected that has a minimal distance between theme (conventionally, particles I and II). Then, one of the two sub-clusters is rotated on the (center of mass–particle I–particle II) plane by an analytically calculated angle to ensure the contact condition. If this does not result in any overlap between the sub-clusters, one obtains a new cluster. Otherwise, the procedure is repeated from the beginning.

As compared to the previous algorithms, there is important distinction. The size characteristic, gyration radius, is recalculated at each generation again using the Huygens–Steiner theorem (13), thus providing higher accuracy with respect to the basic Equation (1). It was clearly shown that an increase in polydispersity within a few tens of percent expands the available D_f range for a given fractal prefactor, and, moreover, there is a k_f interval which allows one to cover the entire fractal dimension range of 1–3 (Figure 13).

Therefore, the generalized model [121] makes it possible to generate clusters with a continuous change in the structure covering an arbitrary wide size scale as well as the full range of fractal dimensions, $1 \leq D_f \leq 3$. The efficient work of the algorithm was demonstrated by the structural analysis of the numerically generated ensembles of clusters in terms of correlation functions (pair distance distribution functions).

The discussed models based on a hierarchical procedure extend the previous studies in this area to the case of the cluster–cluster agglomeration and make it possible to generate clusters with a continuous structural change, covering the full range of natural mass fractal dimensions in three-dimensional space. At a certain iteration two sub-clusters can be aggregated in many ways, each of these ways is associated with the distance between the centers

of mass, which ensures the preservation of both D_f and k_f. Therefore, one needs to apply one scalar constraint on the coordinates of the sub-clusters to satisfy the basic Equation (1). The remaining unbound degrees of freedom ensure a high degree of stochasticity of the aggregates, thus bringing them closer to the objects observed in experiments.

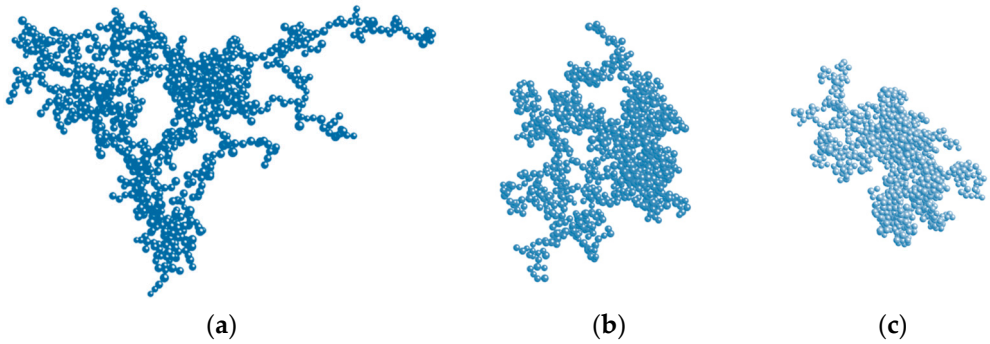

Figure 13. Examples of fractal clusters of 1000 polydisperse particles (log-normal distribution, polydispersity 10%) simulated by the generalized algorithm with different fractal dimensions: $D_f = 1.5$ (**a**), $D_f = 2.0$ (**b**), $D_f = 2.5$ (**c**). Adapted with permission from ref. [121]. 2020, Elsevier.

2.5. Fractal Chains

The dynamics of macromolecules in solution, governed by their self-similar chain structure, serves as the foundation for molecular characterization. The accurate interpretation of experimental measurements enables the determination of the polymer structure in solution [7]. A robust algorithm for constructing fractal chains was proposed and analyzed in a full range of fractal dimensions, $1 \leq D_f \leq 3$ (Figure 14) [143,144].

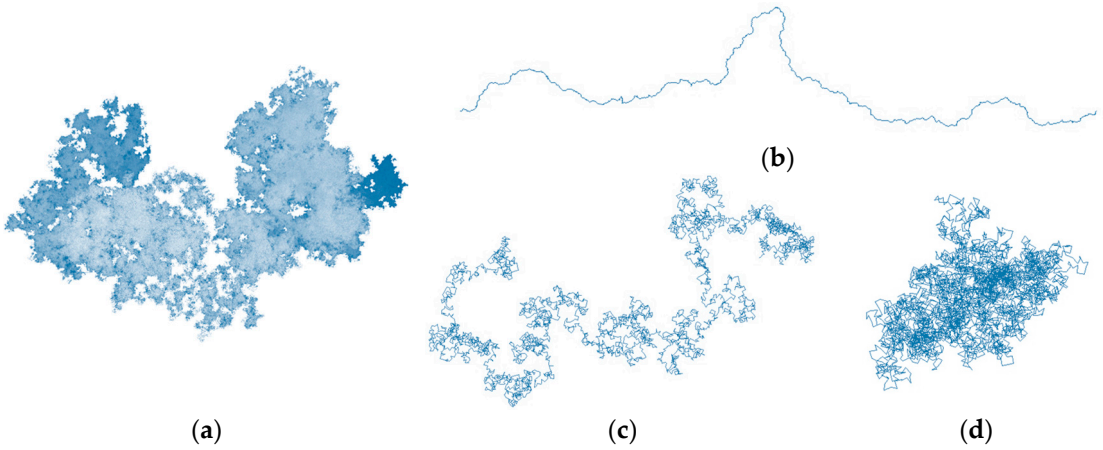

Figure 14. Model stochastic fractal chains with various fractal dimensions: $D_f = 2.4$ (**a**) [143], $D_f = 1.1$ (**b**), $D_f = 2.0$ (**c**), $D_f = 2.9$ (**d**). Adapted with permission from ref. [144]. 2019, AIP Publishing.

One of the methods to generate fractals is self-similarity transformation like in a case of the Koch curve [1,145]. It is the fractal of topological dimension 1. At the beginning, the fractal initiator is a line segment of length L. Then, the initiator is replaced by a generator that is a broken line of i intervals of length L/f, thus producing a fractal of the first generation. Each interval of the generator is replaced by the whole generator at the next steps. A fractal of the j-th order consists of i^j intervals of length L/f^j. For an ideal fractal obtained using this procedure in the limit $j \to \infty$, the fractal dimension is defined as the similarity dimension [1]:

$$D_f = \ln(i)/\ln(f). \quad (15)$$

Regular fractals in the style of the Koch curve have additional types of symmetry that affect the correlation properties and make it difficult to determine the D_f parameter via Equation (2) [143]. However, if the generator is randomly changed at each step of generation under constant i and f, then an irregular fractal will be built for large but finite j [143]. Several spectacular examples are given in Figure 14. The model can approximate a polymer chain or a fractal cluster if nanoparticles are placed at the vertices of this polygonal line.

2.6. Some Exotic Examples in One Line

2.6.1. Möbius Fractal

As noted, the deterministic fractal aggregation algorithm is based on an exact repetition of the shape at different scales, while when using the stochastic fractal, the scaling ratios are observed only "on average". The proposed algorithm for constructing a fractal object, called the Möbius fractal, is essentially on the verge between regular and non-regular fractals [146]. This model is an example of a stochastic fractal built according to a deterministic protocol without randomization steps. The main idea is to use the Möbius function, $\mu(x)$, the values of which change in a quasi-random way, but the function itself is unambiguous [147]. It is defined on the set of natural numbers, $x \in \mathbb{N}$, and takes values -1, 0 and 1 depending on factorization of x into prime factors. The values of the $\mu(x)$ function are associated with the left/straight/right directions of movement on a square lattice. Thus, an arbitrarily large topologically linear fractal can be constructed but with a fractal dimension greater than 1 (Figure 15a). According to the correlation analysis, the fractal dimension of such a system is close to 1.75. Cluster size variation as well as structural diversity can be easily achieved using different input x ranges.

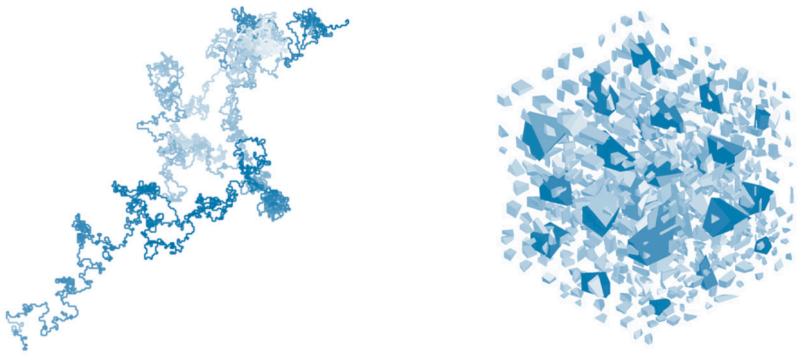

(**a**) (**b**)

Figure 15. (**a**) Möbius fractal for $N = 5000$ unique vertices. Adapted with permission from ref. [146]. 2021, AIP Publishing. (**b**) An illustration of the three-dimensional Yang and Wang model. A single cell of the cube processed is shown to explain the algorithm. Adapted with permission from ref. [148]. 2015, Elsevier.

2.6.2. Modeling Method Based on the Menger Sponge

Yang and Wang describes a generating algorithm [148], based on the random geometrical fractal approach, for simulating mesostructured aggregates. The modified model was introduced for approximating the actual state, with the assumption that the particular models are randomly convex hexahedral in three-dimensional space (Figure 15b). The fractal dimension was estimated at a level of 2.6153, close enough to the value of 2.7268 for the deterministic Menger sponge model underlying the considered algorithm [1,149].

2.6.3. Dynamic Lattice Liquid Model

The Dynamic Lattice Liquid model was proposed as a tool for studying various aggregation processes [150]. This model allows for the performance of simulations of systems with a constant number of particles and explicit solvent presence. It is based on a lattice structure with particles located at all lattice sites. They cannot move individually. However, a long-range cooperative mobility in such system can take place in the form of

multiparticle movement in closed loops. To simulate fractal aggregation, it is assumed that two types of particles are randomly distributed in the system. One particle type is capable of aggregation when meeting similar (dispersed) particles, while the other is not (solvent). The Dynamic Lattice Liquid algorithm properly reflects structural and dynamic properties of the stochastic fractal growth process (Figure 16). With this approach, the resulting fractal dimension lies in the range of $1.7 \leq D_f \leq 2$ and is clearly correlated with the initial concentration of dispersed particles, which is in good agreement with the predictions based on Smoluchowski equation for DLCA.

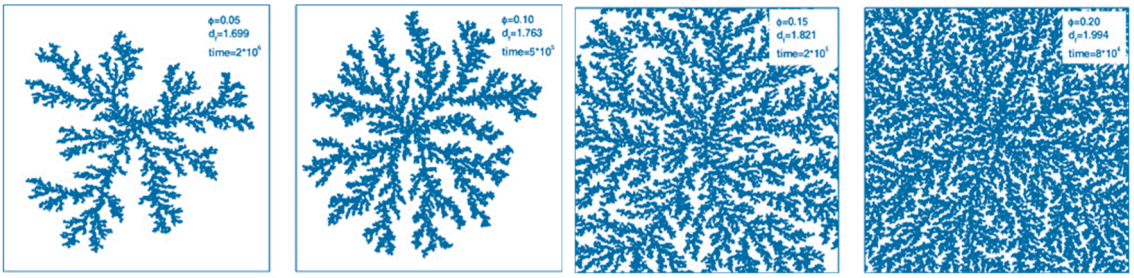

Figure 16. Dynamic Lattice Liquid structures at the same scale depending on the initial concentration. Initial concentration, fractal dimension, and growing time are indicated in the figures. Adapted with permission from ref. [150]. 2007, Elsevier.

The Monte Carlo methods are unable to capture structural changes influenced by the interplay of kinetic processes, such as simultaneous aggregation, coalescence or restructuring. Additionally, they do not yield a time-dependent evolution of the fractal dimension. Monte Carlo simulations also encounter constraints when attempting to model aggregation processes involving interactions beyond the scope of potential functions, including hydrodynamic effects like shear-induced aggregation and hydrodynamic interactions. Notwithstanding these limitations, the aggregates generated by these methods remain useful for computing various physical and mechanical properties. For instance, thermal and electrical conductivities, as well as elastic and optical properties, present suitable options for further calculation using these aggregates.

3. Concluding Remarks

Summarizing, the fractal cluster concept has proven to be a suitable approach for describing the aggregation of colloids, aerosols, etc. A comparison between computer simulations and experiments has helped to elucidate the underlying mechanisms of real aggregation processes. Stochastic models of fractal growth have inspired plenty of studies and applications in physics, biology, chemistry, material science, nanotechnology, biomedicine, and other domains containing disordered, at first glance, systems. Overall, the studies provide important insights into the properties of disordered fractal aggregates and their behavior under different conditions.

This review has highlighted recent advances in developing a comprehensive understanding of the formation, structure and properties of fractal aggregates, with a major emphasis on the contributions of computer simulations. The generation algorithms able to realize fractal dimensions in a final structure according to preset values have been described, along with realistic extensions that can reproduce specific experimental results.

The article has focused solely on the geometrical structure of fractal-like objects and the role of different parameters in defining models of aggregation. The current state of modeling includes push-button methods with a variety of input parameters. These trends are expected to continue in the future, leading to increasingly realistic models for colloidal aggregation processes and a better understanding of the basic models presented in this review. The methods reviewed may find wide applications far beyond colloid science, given the current popularity of fractals in miscellaneous disciplines. Each of the presented classes of models has its own pros and cons regarding the reproduction of aggregation

kinetics, the coverage of the range of fractal dimension values, or the rate of structure generation. Hence, this review can serve as a guide for finding an appropriate generating algorithm that can describe specific experimental observations.

Funding: This research received no external funding.

Data Availability Statement: Not applicable.

Acknowledgments: The author greatly appreciates discussions with Leonid Bulavin (Taras Shevchenko National University of Kyiv) and Wojciech Zając (Institute of Nuclear Physics PAS).

Conflicts of Interest: The author declares no conflict of interest.

References

1. Mandelbrot, B.B. *The Fractal Geometry of Nature*; W. H. Freeman and Co.: San Francisco, CA, USA, 1982; 460p.
2. Sander, L.M. Fractal growth processes. *Nature* **1986**, *322*, 789–793. [CrossRef]
3. Pfeifer, P. Fractal dimension as working tool for surface-roughness problems. *Appl. Surf. Sci.* **1984**, *18*, 146–164. [CrossRef]
4. Timmons, J.; Falzone, G.; Balonis, M.; Bauchy, M.; Sant, G. Anomalous variations in the viscous activation energy of suspensions induced by fractal structuring. *J. Colloid Interface Sci.* **2018**, *530*, 603–609. [CrossRef] [PubMed]
5. Lesin, V.I.; Koksharov, Y.A.; Khomutov, G.B. Viscosity of liquid suspensions with fractal aggregates: Magnetic nanoparticles in petroleum colloidal structures. *Colloids Surf. A Physicochem. Eng. Asp.* **2011**, *392*, 88–94. [CrossRef]
6. Meakin, P. Fractal aggregates in geophysics. *Rev. Geophys.* **1991**, *29*, 317–354. [CrossRef]
7. Gmachowski, L. Fractal aggregate model of chain with mixed statistics. *Polymer* **2007**, *48*, 4316–4321. [CrossRef]
8. Feder, J. *Fractals*; Plenum Press: New York, NY, USA, 1988; 284p.
9. Maximova, N.; Dahl, O. Environmental implications of aggregation phenomena: Current understanding. *Curr. Opin. Colloid Interface Sci.* **2006**, *11*, 246–266. [CrossRef]
10. Xu, P.; Mujumdar, A.S.; Yu, B. Fractal theory on drying: A review. *Dry. Technol.* **2008**, *26*, 640–650. [CrossRef]
11. Pratsinis, S.E. Flame aerosol synthesis of ceramic powders. *Prog. Energy Combust. Sci.* **1998**, *24*, 197–219. [CrossRef]
12. Kim, M.Y.; Park, S.H. A numerical aerosol model Fractal Aggregate Moment Model (FAMM) to simulate simultaneous nucleation, coagulation, surface growth, and sintering of fractal aggregates. *Aerosol Sci. Technol.* **2019**, *53*, 493–507. [CrossRef]
13. Weisenstein, D.K.; Keith, D.W.; Dykema, J.A. Solar geoengineering using solid aerosol in the stratosphere. *Atmos. Chem. Phys.* **2015**, *15*, 11835–11859. [CrossRef]
14. Yang, X.; Wang, F.; Yang, X.; Zhou, Q. Fractal dimension in concrete and implementation for meso-simulation. *Constr. Build. Mater.* **2017**, *143*, 464–472. [CrossRef]
15. Smith, T.G., Jr.; Lange, G.D.; Marks, W.B. Fractal methods and results in cellular morphology—Dimensions, lacunarity and multifractals. *J. Neurosci. Methods* **1996**, *69*, 123–136. [CrossRef] [PubMed]
16. Sosnowski, T.R. Nanosized and nanostructured particles in pulmonary drug delivery. *J. Nanosci. Nanotechnol.* **2015**, *15*, 3476–3487. [CrossRef] [PubMed]
17. Oświęcimka, P.; Kwapień, J.; Drozdz, S. Multifractality in the stock market: Price increments versus waiting times. *Phys. A* **2005**, *347*, 626–638. [CrossRef]
18. Schaefer, D.W.; Martin, J.E.; Wiltzius, P.; Cannell, D.S. Fractal geometry of colloidal aggregates. *Phys. Rev. Lett.* **1984**, *52*, 2371–2374. [CrossRef]
19. Lazzari, S.; Nicoud, L.; Jaquet, B.; Lattuada, M.; Morbidelli, M. Fractal-like structures in colloid science. *Adv. Colloid Interface Sci.* **2016**, *235*, 1–13. [CrossRef]
20. Dickinson, E. Structure and rheology of colloidal particle gels: Insight from computer simulation. *Adv. Colloid Interface Sci.* **2013**, *199–200*, 114–127. [CrossRef]
21. Eggersdorfer, M.L.; Pratsinis, S.E. The structure of agglomerates consisting of polydisperse particles. *Aerosol Sci. Technol.* **2012**, *46*, 347–353. [CrossRef]
22. Morán, J.; Yon, J.; Poux, A. Monte Carlo Aggregation Code (MCAC) Part 1: Fundamentals. *J. Colloid Interface Sci.* **2020**, *569*, 184–194. [CrossRef]
23. Beeckmans, J.M. The density of aggregated solid aerosol particles. *Ann. Occup. Hyg.* **1964**, *7*, 299–305. [CrossRef]
24. Meakin, P. Fractal Aggregates. *Adv. Colloid Interface Sci.* **1987**, *28*, 249–331. [CrossRef] [PubMed]
25. Mandelbrot, B.B. Measures of fractal lacunarity: Minkowski content and alternatives. In *Fractal Geometry and Stochastics. Progress in Probability*; Bandt, C., Graf, S., Zähle, M., Eds.; Birkhäuser: Basel, Switzerland, 1995; Volume 37, pp. 15–42.
26. Tomchuk, O.V.; Bulavin, L.A.; Pipich, V.; Ryukhtin, V.; Ivankov, O.I.; Aksenov, V.L.; Avdeev, M.V. Fractal aggregation in silica sols in basic tetraethoxysilane/ethanol/water solutions by small-angle neutron scattering. *J. Mol. Liq.* **2020**, *304*, 112736. [CrossRef]
27. Bushell, G.C.; Yan, Y.D.; Woodfield, D.; Raper, J.; Amal, R. On techniques for the measurement of the mass fractal dimension of aggregates. *Adv. Colloid Interface Sci.* **2002**, *95*, 1–50. [CrossRef] [PubMed]
28. Anitas, E.M. *Small-Angle Scattering (Neutrons, X-rays, Light) from Complex Systems. Fractal and Multifractal Models for Interpretation of Experimental Data*; Springer: Cham, Switzerland, 2019; 116p. [CrossRef]

29. Beaucage, G. Determination of branch fraction and minimum dimension of mass-fractal aggregates. *Phys. Rev. E* **2004**, *70*, 031401. [CrossRef] [PubMed]
30. Besselink, R.; Stawski, T.M.; Van Driessche, A.E.S.; Benning, L.G. Not just fractal surfaces, but surface fractal aggregates: Derivation of the expression for the structure factor and its applications. *J. Chem. Phys.* **2016**, *145*, 211908. [CrossRef]
31. Tence, M.; Chevalier, J.P.; Jullien, R. On the measurement of the fractal dimension of aggregated particles by electron microscopy: Experimental method, corrections and comparison with numerical models. *J. Phys.* **1986**, *47*, 1989–1998. [CrossRef]
32. Dastanpour, R.; Boone, J.M.; Rogak, S.N. Automated primary particle sizing of nanoparticle aggregates by TEM image analysis. *Powder Technol.* **2016**, *295*, 218–224. [CrossRef]
33. Kütz, S.; Schmidt-Ott, A. Use of a low-pressure impactor for fractal analysis of submicron particles. *J. Aerosol Sci.* **1990**, *21*, S47–S50. [CrossRef]
34. Schmidt-Ott, A.; Baltensperger, U.; Gaggeler, H.W.; Jost, D.T. Scaling behaviour of physical parameters describing agglomerates. *J. Aerosol Sci.* **1990**, *21*, 711–717. [CrossRef]
35. Magill, J. Fractal dimension and aerosol particle dynamics. *J. Aerosol Sci.* **1991**, *22*, S165–S168. [CrossRef]
36. Wu, H.; Morbidelli, M. A model relating structure of colloidal gels to their elastic properties. *Langmuir* **2001**, *17*, 1030–1036. [CrossRef]
37. Pfeifer, P.; Avnir, D. Chemistry in noninteger dimensions between two and three. I. Fractal theory of heterogeneous surfaces. *J. Chem. Phys.* **1983**, *79*, 3558–3565. [CrossRef]
38. Avnir, D.; Farin, D.; Pfeifer, P. Chemistry in noninteger dimensions between two and three. II. Fractal surfaces of adsorbents. *J. Chem. Phys.* **1983**, *79*, 3566–3571. [CrossRef]
39. Heinson, W.R.; Sorensen, C.M.; Chakrabarti, A. A three parameter description of the structure of diffusion limited cluster fractal aggregates. *J. Colloid Interface Sci.* **2012**, *375*, 65–69. [CrossRef] [PubMed]
40. Yon, J.; Morán, J.; Ouf, F.-X.; Mazur, M.; Mitchell, J.B. From monomers to agglomerates: A generalized model for characterizing the morphology of fractal-like clusters. *J. Aerosol Sci.* **2021**, *151*, 105628. [CrossRef]
41. Morán, J.; Henry, C.; Poux, A.; Yon, J. Impact of the maturation process on soot particle aggregation kinetics and morphology. *Carbon* **2021**, *182*, 837–846. [CrossRef]
42. Witten, T.A.; Sander, L.M. Diffusion-limited aggregation, a kinetic critical phenomenon. *Phys. Rev. Lett.* **1981**, *47*, 1400–1403. [CrossRef]
43. Witten, T.A.; Sander, L.M. Diffusion-limited aggregation. *Phys. Rev. B.* **1983**, *27*, 5686–5697. [CrossRef]
44. Meakin, P. Formation of fractal clusters and networks by irreversible diffusion-limited aggregation. *Phys. Rev. Lett.* **1983**, *51*, 1119–1122. [CrossRef]
45. Meakin, P. Off lattice simulations of cluster-cluster aggregation in dimensions 2–6. *Phys. Lett. A* **1985**, *107*, 269–272. [CrossRef]
46. Brasil, A.M.; Farias, T.L.; Carvalho, M.G. Evaluation of the fractal properties of cluster–cluster aggregates. *Aerosol Sci. Technol.* **2000**, *33*, 440–454. [CrossRef]
47. Kolb, M.; Botet, R.; Jullien, R. Scaling of kinetically growing clusters. *Phys. Rev. Lett.* **1983**, *51*, 1123–1126. [CrossRef]
48. Brown, W.D.; Ball, R.C. Computer simulation of chemically limited aggregation. *J. Phys. A Math. Gen.* **1985**, *18*, L517–L521. [CrossRef]
49. Jullien, R.; Kolb, M. Hierarchical model for chemically limited clustercluster aggregation. *J. Phys. A Math. Gen.* **1984**, *17*, L639–L643. [CrossRef]
50. Kolb, M.; Jullien, R. Chemically limited versus diffusion limited aggregation. *J. Phys. Lett.* **1984**, *45*, L977–L981. [CrossRef]
51. Ball, R.C.; Jullien, R. Finite size effects in cluster-cluster aggregation. *J. Phys. Lett.* **1984**, *45*, 1031–1035. [CrossRef]
52. Meakin, P.; Jullien, R. The effects of restructuring on the geometry of clusters formed by diffusion-limited, ballistic, and reaction-limited cluster-cluster aggregation. *J. Chem. Phys.* **1988**, *89*, 246–250. [CrossRef]
53. Viglis, T.A. Flory theory of polymeric fractals—Intersection, saturation and condensation. *Phys. A* **1988**, *153*, 341–354. [CrossRef]
54. Malcai, O.; Lidar, D.A.; Biham, O. Scaling range and cutoffs in empirical fractals. *Phys. Rev. E* **1997**, *56*, 2817–2828. [CrossRef]
55. Tomchuk, O.V. Fractal concept in structural analysis of nanosystems: A retrospective look and prospects. *Ukr. J. Phys.* **2020**, *65*, 709–728. [CrossRef]
56. Voss, R.F. Multiparticle fractal aggregation. *J. Stat. Phys.* **1984**, *36*, 861–872. [CrossRef]
57. Jullien, R.; Botet, R.; Mors, P.M. Computer simulations of cluster-cluster aggregation. *Faraday Discuss. Chem. Soc.* **1987**, *83*, 125–137. [CrossRef]
58. Botet, R.; Jullien, R. Fractal aggregates of particles. *Ph. Transit.* **1990**, *24–26*, 691–736. [CrossRef]
59. Jullien, R. The application of fractals to colloidal aggregation. *Croat. Chem. Acta* **1992**, *65*, 215–235.
60. Meakin, P. A Historical introduction to computer models for fractal aggregates. *J. Sol-Gel Sci. Technol.* **1999**, *15*, 97–117. [CrossRef]
61. Meakin, P. Effects of cluster trajectories on cluster-cluster aggregation: A comparison of linear and Brownian trajectories in two- and three-dimensional simulations. *Phys. Rev. A* **1984**, *29*, 997–999. [CrossRef]
62. Avdeev, M.V.; Aksenov, V.L.; Rosta, L. Pressure induced changes in fractal structure of detonation nanodiamond powder by small-angle neutron scattering. *Diam. Relat. Mater.* **2007**, *16*, 2050–2053. [CrossRef]
63. Tomchuk, O.V.; Avdeev, M.V.; Aksenov, V.L.; Shulenina, A.V.; Ivankov, O.I.; Ryukhtin, V.; Vékás, L.; Bulavin, L.A. Temperature-dependent fractal structure of particle clusters in aqueous ferrofluids by small-angle scattering. *Colloids Surf. A Physicochem. Eng. Asp.* **2021**, *613*, 126090. [CrossRef]

64. Chakraborti, R.K.; Gardner, K.H.; Atkinson, J.F.; van Benschoten, J.E. Changes in fractal dimension during aggregation. *Water Res.* **2003**, *37*, 873–883. [CrossRef]
65. Deng, L.; Wang, Y.-T.; Ou-Yang, Z.-C. Diffusion-limited aggregation with polygon particles. *Commun. Theor. Phys.* **2012**, *58*, 895–901. [CrossRef]
66. Farias, T.L.; Köylü, Ü.Ö.; Carvalho, M.G. Effects of polydispersity of aggregates and primary particles on radiative properties of simulated soot. *J. Quant. Spectrosc. Radiat. Transf.* **1996**, *55*, 357–371. [CrossRef]
67. Hasmy, A.; Vacher, R.; Jullien, R. Small-angle scattering by fractal aggregates: A numerical investigation of the crossover between the fractal regime and the Porod regime. *Phys. Rev. B* **1994**, *50*, 1305–1308. [CrossRef]
68. Goudeli, E.; Eggersdorfer, M.L.; Pratsinis, S.E. Coagulation of agglomerates consisting of polydisperse primary particles. *Langmuir* **2016**, *32*, 9276–9285. [CrossRef] [PubMed]
69. Tenti, J.M.; Hernández Guiance, S.N.; Irurzun, I.M. Fractal dimension of diffusion-limited aggregation clusters grown on spherical surfaces. *Phys. Rev. E* **2021**, *103*, 012138. [CrossRef] [PubMed]
70. Wang, R.; Singh, A.K.; Kolan, S.R.; Tsotsas, E. Fractal analysis of aggregates: Correlation between the 2D and 3D box-counting fractal dimension and power law fractal dimension. *Chaos Solitons Fractals* **2022**, *160*, 112246. [CrossRef]
71. Schmidt, P.W. Small-angle scattering studies of disordered, porous and fractal systems. *J. Appl. Cryst.* **1991**, *24*, 414–435. [CrossRef]
72. Cherny, A.Y.; Anitas, E.M.; Kuklin, A.I.; Balasoiu, M.; Osipov, V.A. Scattering from generalized Cantor fractals. *J. Appl. Cryst.* **2010**, *43*, 790–797. [CrossRef]
73. Cherny, A.Y.; Anitas, E.M.; Osipov, V.A.; Kuklin, A.I. Deterministic fractals: Extracting additional information from small-angle scattering data. *Phys. Rev. E* **2011**, *84*, 036203. [CrossRef]
74. Kryven, I.; Lazzari, S.; Storti, G. Population balance modeling of aggregation and coalescence in colloidal systems. *Macromol. Theory Simul.* **2014**, *23*, 170–181. [CrossRef]
75. Rigopoulos, S. Population balance modelling of polydispersed particles in reactive flows. *Prog. Energy Combust. Sci.* **2010**, *36*, 412–443. [CrossRef]
76. Kim, J.; Kramer, T.A. Improved orthokinetic coagulation model for fractal colloids: Aggregation and breakup. *Chem. Eng. Sci.* **2006**, *61*, 45–53. [CrossRef]
77. Kostoglou, M.; Konstandopoulos, A.G.; Friedlander, S.K. Bivariate population dynamics simulation of fractal aerosol aggregate coagulation and restructuring. *J. Aerosol Sci.* **2006**, *37*, 1102–1115. [CrossRef]
78. Jeldres, R.I.; Fawell, P.D.; Florio, B.J. Population balance modelling to describe the particle aggregation process: A review. *Powder Technol.* **2018**, *326*, 190–207. [CrossRef]
79. Ansell, G.C.; Dickinson, E. Short-range structure of simulated colloidal aggregates. *Phys. Rev. A* **1987**, *35*, 2349–2352. [CrossRef] [PubMed]
80. Phung, T.N.; Brady, J.F.; Bossis, G. Stokesian Dynamics simulation of Brownian suspensions. *J. Fluid Mech.* **1996**, *313*, 181–207. [CrossRef]
81. Sierou, A.; Brady, J.F. Accelerated Stokesian Dynamics simulations. *J. Fluid Mech.* **2001**, *448*, 115–146. [CrossRef]
82. Whittle, M.; Dickinson, E. Brownian dynamics simulation of gelation in soft sphere systems with irreversible bond formation. *Mol. Phys.* **1997**, *90*, 739–757. [CrossRef]
83. Ermak, D.L.; McCammon, J.A. Brownian dynamics with hydrodynamic interactions. *J. Chem. Phys.* **1978**, *69*, 1352–1360. [CrossRef]
84. Heyes, D.M.; Mitchell, P.J. Mean-field hydrodynamics brownian dynamics simulations of stabilized colloidal liquids under shear. *J. Non-Newton. Fluid. Mech.* **1997**, *68*, 101–124. [CrossRef]
85. Groot, R.D.; Warren, P.B. Dissipative particle dynamics: Bridging the gap between atomistic and mesoscopic simulation. *J. Chem. Phys.* **1997**, *107*, 4423–4435. [CrossRef]
86. Español, P.; Warren, P.B. Statistical mechanics of Dissipative Particle Dynamics. *Europhys. Lett.* **1995**, *30*, 191–196. [CrossRef]
87. Ferri, G.; Humbert, S.; Digne, M.; Schweitzer, J.-M.; Moreaud, M. Simulation of large aggregate particles system with a new morphological model. *Image Anal. Stereol.* **2021**, *40*, 71–84. [CrossRef]
88. Mountain, R.D.; Mulholland, G.W.; Baum, H. Simulation of aerosol agglomeration in the free molecular and continuum flow regimes. *J. Colloid Interface Sci.* **1986**, *114*, 67–81. [CrossRef]
89. Meakin, P. Cluster-particle aggregation with fractal (Levy flight) particle trajectories. *Phys. Rev. B* **1984**, *29*, 3722–3725. [CrossRef]
90. Jungblut, S.; Joswig, J.-O.; Eychmüller, A. Diffusion- and reaction-limited cluster aggregation revisited. *Phys. Chem. Chem. Phys.* **2019**, *21*, 5723–5729. [CrossRef] [PubMed]
91. Meakin, P. Structural readjustment effects in cluster-cluster aggregation. *J. Phys.* **1985**, *46*, 1543–1552. [CrossRef]
92. Jullien, R.; Hasmy, A. Fluctuating bond aggregation: A model for chemical gel formation. *Phys. Rev. Lett.* **1995**, *74*, 4003–4006. [CrossRef]
93. Jullien, R. A new model of cluster aggregation. *J. Phys. A Math. Gen.* **1986**, *19*, 2129–2136. [CrossRef]
94. Mors, P.M.; Botet, R.; Jullien, R. Cluster-cluster aggregation with dipolar interactions. *J. Phys. A Math. Gen.* **1987**, *20*, L975–L980. [CrossRef]
95. Jullien, R.; Meakin, P. Simple models for the restructuring of three-dimensional ballistic aggregates. *J. Colloid Interface Sci.* **1989**, *127*, 265–272. [CrossRef]

96. Oh, C.; Sorensen, C.M. The effect of overlap between monomers on the determination of fractal cluster morphology. *J. Colloid Interface Sci.* **1997**, *193*, 17–25. [CrossRef]
97. Meakin, P. The effects of rotational diffusion on the fractal dimensionality of structures formed by cluster–cluster aggregation. *J. Chem. Phys.* **1984**, *81*, 4637–4639. [CrossRef]
98. Loskutov, A.; Andrievsky, D.; Ivanov, V.; Vasiliev, K.; Ryabov, A. Fractal growth of rotating DLA-clusters. *Macromol. Symp.* **2000**, *160*, 239–248. [CrossRef]
99. Kim, S.; Lee, K.-S.; Zachariah, M.R.; Lee, D. Three-dimensional off-lattice Monte Carlo simulations on a direct relation between experimental process parameters and fractal dimension of colloidal aggregates. *J. Colloid Interface Sci.* **2010**, *344*, 353–361. [CrossRef]
100. Heinson, W.R.; Pierce, F.; Sorensen, C.M.; Chakrabarti, A. Crossover from ballistic to epstein diffusion in the free-molecular regime. *Aerosol Sci. Technol.* **2014**, *48*, 738–746. [CrossRef]
101. Goudeli, E.; Eggersdorfer, M.L.; Pratsinis, S.E. Coagulation−agglomeration of fractal-like particles: Structure and self-preserving size distribution. *Langmuir* **2015**, *31*, 1320–1327. [CrossRef] [PubMed]
102. Hayashi, S.; Hisaeda, Y.; Asakuma, Y.; Aoki, H.; Miura, T.; Yano, H.; Sawa, Y. Simulation of soot aggregates formed by benzene pyrolysis. *Combust. Flame* **1999**, *117*, 851–860. [CrossRef]
103. Camejo, M.D.; Espeso, D.R.; Bonilla, L.L. Influence of primary-particle density in the morphology of agglomerates. *Phys. Rev. E* **2014**, *90*, 012306. [CrossRef] [PubMed]
104. Morán, J.; Yon, J.; Poux, A.; Corbin, F.; Ouf, F.-X.; Siméon, A. Monte Carlo Aggregation Code (MCAC) Part 2: Application to soot agglomeration, highlighting the importance of primary particles. *J. Colloid Interface Sci.* **2020**, *575*, 274–285. [CrossRef] [PubMed]
105. Paoluzzi, M.; Leoni, M.; Marchetti, M.C. Fractal aggregation of active particles. *Phys. Rev. E* **2018**, *98*, 052603. [CrossRef]
106. Nicolás-Carlock, J.R.; Carrillo-Estrada, J.L.; Dossetti, V. Fractality *à la carte*: A general particle aggregation model. *Sci. Rep.* **2016**, *6*, 19505. [CrossRef] [PubMed]
107. Hurd, A.J.; Schaeffer, D.W. Diffusion-limited aggregation in two dimensions. *Phys. Rev. Lett.* **1985**, *54*, 1043–1046. [CrossRef] [PubMed]
108. Jullien, R. Transparency effects in cluster-cluster aggregation with linear trajectories. *J. Phys. A Math. Gen.* **1984**, *17*, L771–L776. [CrossRef]
109. Eden, M. A two-dimensional growth process. In Proceedings of the Fourth Berkeley Symposium on Mathematical Statistics and Probability, Berkeley, CA, USA, 20 June–30 July 1960; Neyman, J., Ed.; University of California Press: Berkeley, LA, USA, 1961; Volume IV, pp. 223–239.
110. Takeuchi, K.A. Statistics of circular interface fluctuations in an off-lattice Eden model. *J. Stat. Mech.* **2012**, *5*, P05007. [CrossRef]
111. Wang, C.Y.; Liu, P.L.; Bassingthwaighte, J.B. Off-lattice Eden-C cluster growth model. *J. Phys. A Math. Gen.* **1995**, *28*, 2141–2147. [CrossRef]
112. Guesnet, E.; Dendievel, R.; Jauffrès, D.; Martin, C.L.; Yrieix, B. A growth model for the generation of particle aggregates with tunable fractal dimension. *Phys. A* **2019**, *513*, 63–73. [CrossRef]
113. Filippov, A.V.; Zurita, M.; Rosner, D.E. Fractal-like aggregates: Relation between morphology and physical properties. *J. Colloid Interface Sci.* **2000**, *229*, 261–273. [CrossRef]
114. Mackowski, D.W. Calculation of total cross sections of multiple-sphere clusters. *J. Opt. Soc. Am. A* **1994**, *11*, 2851–2861. [CrossRef]
115. Mackowski, D.W. Electrostatics analysis of radiative absorption by sphere clusters in the Rayleigh limit: Application to soot particles. *Appl. Opt.* **1995**, *34*, 3535–3545. [CrossRef]
116. Singh, A.K.; Tsotsas, E. A tunable aggregation model incorporated in Monte Carlo simulations of spray fluidized bed agglomeration. *Powder Technol.* **2020**, *364*, 417–428. [CrossRef]
117. Dolotov, S.V.; Roldughin, V.I. Simulation of ESR spectra of metal nanoparticle aggregates. *Colloid J.* **2007**, *69*, 9–12. [CrossRef]
118. Tomchuk, O.V.; Volkov, D.S.; Bulavin, L.A.; Rogachev, A.V.; Proskurnin, M.A.; Korobov, M.V.; Avdeev, M.V. Structural characteristics of aqueous dispersions of detonation nanodiamond and their aggregate fractions by small-angle neutron scattering. *J. Phys. Chem. C* **2015**, *119*, 794–802. [CrossRef]
119. Singh, A.K.; Tsotsas, E. A Fast and improved tunable aggregation model for stochastic simulation of spray fluidized bed agglomeration. *Energies* **2021**, *14*, 7221. [CrossRef]
120. Sorensen, C.M.; Roberts, G.C. The prefactor of fractal aggregates. *J. Colloid Interface Sci.* **1997**, *186*, 447–452. [CrossRef]
121. Tomchuk, O.V.; Avdeev, M.V.; Bulavin, L.A. Modeling fractal aggregates of polydisperse particles with tunable dimension. *Colloids Surf. A Physicochem. Eng. Asp.* **2020**, *605*, 125331. [CrossRef]
122. Ehrl, L.; Soos, M.; Lattuada, M. Generation and geometrical analysis of dense clusters with variable fractal dimension. *J. Phys. Chem. B* **2009**, *113*, 10587–10599. [CrossRef]
123. Gmachowski, L. Calculation of the fractal dimension of aggregates. *Colloids Surf. A Physicochem. Eng. Asp.* **2002**, *211*, 197–203. [CrossRef]
124. Singh, A.K.; Tsotsas, E. Stochastic model to simulate spray fluidized bed agglomeration: A morphological approach. *Powder Technol.* **2019**, *355*, 449–460. [CrossRef]
125. Bushell, G.; Amal, R. Fractal aggregates of polydisperse particles. *J. Colloid Interface Sci.* **1998**, *205*, 459–469. [CrossRef]
126. Bushell, G.; Amal, R.; Raper, J. The effect of polydispersity in primary particle size on measurement of the fractal dimension of aggregates. *Part. Part. Syst. Charact.* **1998**, *15*, 3–8. [CrossRef]

127. Kowalczyk, P.; Piña-Salazar, E.-Z.; Kirkensgaard, J.J.K.; Terzyk, A.P.; Futamura, R.; Hayashi, T.; Ōsawa, E.; Kaneko, K.; Ciach, A. Reconstructing the fractal clusters of detonation nanodiamonds from small-angle X-ray scattering. *Carbon* **2020**, *169*, 349–356. [CrossRef]
128. Tan, Z.-J.; Zou, X.-W.; Zhang, W.-B.; Jin, Z.-Z. Influence of particle size on diffusion-limited aggregation. *Phys. Rev. E* **1999**, *60*, 6202–6205. [CrossRef] [PubMed]
129. Braga, F.L.; Mattos, O.A.; Amorina, V.S.; Souza, A.B. Diffusion limited aggregation of particles with different sizes: Fractal dimension change by anisotropic growth. *Phys. A* **2015**, *429*, 28–34. [CrossRef]
130. Kätzel, U.; Bedrich, R.; Stintz, M.; Ketzmerick, R.; Gottschalk-Gaudig, T.; Barthel, H. Dynamic light scattering for the characterization of polydisperse fractal systems: I. Simulation of the diffusional behavior. *Part. Part. Syst. Charact.* **2008**, *25*, 9–18. [CrossRef]
131. Kätzel, U.; Vorbau, M.; Stintz, M.; Gottschalk-Gaudig, T.; Barthel, H. Dynamic light scattering for the characterization of polydisperse fractal systems: II. Relation between structure and DLS results. *Part. Part. Syst. Charact.* **2008**, *25*, 19–30. [CrossRef]
132. Wang, Y.; Maurel, G.; Couty, M.; Detcheverry, F.; Merabia, S. Implicit medium model for fractal aggregate polymer nanocomposites: Linear viscoelastic properties. *Macromolecules* **2019**, *52*, 2021–2032. [CrossRef]
133. Karagiannakis, N.P.; Skouras, E.D.; Burganos, V.N. Modelling thermal conduction in polydispersed and sintered nanoparticle aggregates. *Nanomaterials* **2022**, *12*, 25. [CrossRef]
134. Singh, A.K.; Tsotsas, E. Influence of polydispersity and breakage on stochastic simulations of spray fluidized bed agglomeration. *Chem. Eng. Sci.* **2022**, *247*, 117022. [CrossRef]
135. Mandelbrot, B.B. Plane DLA is not self-similar; is it a fractal that becomes increasingly compact as it grows? *Phys. A* **1992**, *191*, 95–107. [CrossRef]
136. Oh, C.; Sorensen, C.M. Structure factor of diffusion-limited aggregation clusters: Local structure and non-self-similarity. *Phys. Rev. E* **1998**, *57*, 784–790. [CrossRef]
137. Skorupski, K.; Mroczka, J.; Wriedt, T.; Riefler, N. A fast and accurate implementation of tunable algorithms used for generation of fractal-like aggregate models. *Phys. A* **2014**, *404*, 106–117. [CrossRef]
138. Thouy, R.; Jullien, R. A cluster-cluster aggregation model with tunable fractal dimension. *J. Phys. A Math. Gen.* **1994**, *27*, 2953–2963. [CrossRef]
139. Thouy, R.; Jullien, R.; Benoit, C. Density of vibrational states of fractal aggregates: Scalar interactions. *J. Non-Cryst. Solids* **1998**, *232–234*, 674–681. [CrossRef]
140. Vormoor, O. Large scale fractal aggregates using the tunable dimension cluster–cluster aggregation. *Comput. Phys. Commun.* **2002**, *144*, 121–129. [CrossRef]
141. Morán, J.; Fuentes, A.; Liu, F.; Yon, J. FracVAL: An improved tunable algorithm of cluster–cluster aggregation for generation of fractal structures formed by polydisperse primary particles. *Comput. Phys. Commun.* **2019**, *239*, 225–237. [CrossRef]
142. Feigin, L.A.; Svergun, D.I. *Structure Analysis by Small-Angle X-ray and Neutron Scattering*; Plenum Press: New York, NY, USA, 1987; 335p.
143. Ilatovskiy, A.V.; Lebedev, D.V.; Filatov, M.V.; Petukhov, M.G.; Isaev-Ivanov, V.V. SANS spectra of the fractal supernucleosomal chromatin structure models. *J. Phys. Conf. Ser.* **2012**, *351*, 012007. [CrossRef]
144. Tomchuk, O.V. Some aspects of small-angle scattering by fractal chains. *AIP Conf. Proceed.* **2019**, *2163*, 020006. [CrossRef]
145. von Koch, H. On a continuous curve without a tangent, obtained by an elementary geometrical construction (Sur une courbe continue sans tangente, obtenue par une construction géométrique élémentaire). *Ark. Mat. Astron. Fys.* **1904**, *1*, 681–702.
146. Tomchuk, O.V. Stochastic fractal by deterministic algorithm: Introducing the Möbius fractal. *AIP Conf. Proceed.* **2021**, *2377*, 020002. [CrossRef]
147. Möbius, A.F. About a special kind of reversal of the series (Über eine besondere art von umkehrung der reihen). *J. Reine Angew. Math.* **1832**, *9*, 105–123.
148. Yang, X.; Wang, F. Random-fractal-method-based generation of meso-model for concrete aggregates. *Powder Technol.* **2015**, *284*, 63–77. [CrossRef]
149. Menger, K. *Dimensionstheorie*; B. G. Teubner: Leipzig, Germany; Berlin, Germany, 1928; 319p.
150. Polanowski, P. Parallel simulation of random fractal growth using dynamic lattice liquid (DLL) model. *J. Non-Cryst. Solids* **2007**, *353*, 4575–4580. [CrossRef]